UNITED NATIONS UNIVERSITY
UNU-GTP
Geothermal Training Programme

Orkustofnun, Grensasvegur 9,
IS-108 Reykjavik, Iceland

Reports 2017
Number 16

# CALCITE SCALING POTENTIAL OF KANGDING GEOTHERMAL FIELD, W-SICHUAN PLATEAU, CHINA

**Li Yiman**
Institute of Geology and Geophysics, Chinese Academy of Sciences
No.19, Beitucheng western Road, Chaoyang District, Beijing
CHINA
*liyiman@mail.iggcas.ac.cn*

## ABSTRACT

High temperature geothermal systems in China are mainly along the Himalaya tectonic zone, which extends from Xinjiang to Tibet, western Sichuan Plateau, and Yunnan. One of the main problems during energy production is calcite scaling. This report presents a general calcite scaling potential assessment of the Kangding geothermal fields in the western Sichuan Plateau. Results show that the reservoir fluid reconstructed is slightly over-saturated with respect to calcite and scaling and sinters have been observed in some of the boreholes or springs. Taking fluid from well BH6 as an example, it is saturated with respect calcite in the reservoir conditions and with boiling at different temperatures, it evolves to over-saturated and precipitates in the pipeline. The boiling depth is evaluated to be about 150 m (not considering $CO_2$ and salinity) and 440 m (considering $CO_2$ and salinity) using the HOLA and WELLSIM programmes, respectively. The calcite scale quantity is calculated with three methods and is about 151-300 kg and the thickness is about 1-3 cm which is almost consistent with the observed thickness in the surface pipeline from the production test. Calcite scale removal and prevention methods are reviewed based on their formation mechanisms and for calcite scaling in the Kangding geothermal field, a probable inhibitor injection from laboratory and a field test is suggested with consideration of the reservoir temperature and fluid chemistry.

## 1. INTRODUCTION

Scaling is one of the main problems during geothermal fluid production and utilization. According to thermodynamics, the solubility of minerals will change due to temperature and pressure variations during production and generally, minerals will precipitate to clog boreholes or pipelines (Atkinson et al., 1991). Silica, calcite and Fe-bearing scales are thought to be the dominant depositions, among which calcite scale always occurs in the first stage of boiling, silica scale forms at the stage of waste water discharge while Fe-bearing scale is related to volcanic gas in the geothermal system (Arnórsson, 1981). What kind of scale will form is greatly dependent on the deep fluid compositions and geochemical processes from the reservoir to the wellhead. Generally, silica scaling always occurs in high-temperature geothermal fields (e.g. Iceland, Philippines, New Zealand, and Turkey) while calcite scaling occurs in low-medium temperature geothermal fields (Izgec et al., 2005; Sigfússon and Gunnarsson, 2011; Villaseñor and Calibugan, 2011; Kaypakoğlu et al., 2012; Wang et al., 2015; Quinao et al., 2017). However, in high-temperature geothermal fields in West China along the Himalaya tectonic zone (e.g.,

Yangbajing, Yangyi, Naqu, Dangxiong, Kangding), calcite scaling is found to be a serious problem. As the first geothermal power plant in China, scale cleaning is done periodically (always 1-2 days) in Yangbajing power plant and due to the serious scaling problem, Naqu power plant was abandoned in 1999. The SINOPEC geothermal well in the West Sichuan plateau was almost totally clogged with calcite scale in less than one week causing its failure (Wang et al., 2015).

In order to avoid or inhibit calcite scaling during production, it is better to understand the dominant mechanism of the scale formation and predict how calcite behaves when the temperature or pressure changes, as well as the depth where scaling is occurring. Based on thermodynamic and experimental studies, several programs have been developed to do the prediction model (e.g., WATCH, SOLVEQ, CHILLER, and PHREEQC) (Arnórsson et al., 1982; Reed et al., 2012; Parkhurst and Appelo, 1999). For example, the WATCH program, VDATA program and Ryznar index are adopted to analyse calcite scaling problems in low-temperature wells in Iceland and the allowable super-saturation before calcite scaling formation is determined to be log(Q/K)=0.36-0.5, which indicates that geothermal fluids can contain 2.3 times more $CaCO_3$ by weight than the theoretical amount (Bai, 1991). The CSI (calcite saturation index) changes during adiabatic boiling in two wells from Iran which were studied using WATCH. The results showed that maximum super-saturation is attained at 180°C due to a sharp increase of carbonate ions by boiling. Periodic mechanical cleaning and inhibitor methods were proposed to deal with the calcite scaling depending on the scaling rate (Rahmani, 2007). The comprehensive calcite precipitation potential of geothermal fluids from various geothermal fields in Iceland and Philippines were assessed to study how the CSI evolves and how mixing affects the CSI for solutions from diluted ones to highly saline and from basaltic to andesitic host rock (Remoroza, 2010). Borehole simulator HOLA can be introduced to study whether boiling takes place, and if it does at what depth to predict the calcite scaling depth range, which is found to vary inversely with wellhead pressure (Pingtsoe, 1992). However, pre-evaluation of scaling potential sometimes does not work well in production due to uncertain reasons and additional work is recommended to improve the understanding of the scaling mechanisms to optimize the calcite scaling management (Quinao et al., 2017). Therefore, both a calcite scaling potential assessment and the possible prevention or removal methods should be proposed when dealing with geothermal fluid with scaling risk before and during production.

Since calcite scaling problems are typical and one of the main obstacles in high-temperature geothermal systems in the Himalaya tectonic zone in West China, how to assess it and what can be done to avoid or inhibit it should be carefully studied. In this report, the WATCH, PHREEQC, HOLA and WELLSIM programmes are used to analyse calcite scaling problems, including the scaling potential with various temperatures, the depth prediction where scaling is possibly occurring, scale quantity and the prevention or removal methods for geothermal fluid both from boreholes and hot springs in West China.

## 2. THERMODYNAMIC PROPERTIES OF $CO_2$

Calcite scaling in geothermal systems is mainly caused by four geochemical processes: (1) degassing of $CO_2$ due to depressurizing of the fluid from the deep reservoir to the wellhead, (2) pH increase caused by casing corrosion, (3) gas influx from the geothermal reservoir and subsequent $CO_2$ stripping from the fluid, and (4) pH increase and $CO_2$ moving into gas phase due to boiling within the borehole (Wanner et al., 2017). Therefore, for most of the calcite scaling conditions, $CO_2$ is a key factor and it is necessary to know how $CO_2$ behaves under various temperatures, pressures and salinity conditions.

### 2.1 The P-T phase diagram of $CO_2$

Based on previous studies on the equation of state for $CO_2$, the critical point and triple point are estimated to be 31°C at 74 bar (Suehiro et al., 1996; Span and Wagner, 1996) and -56.57±0.03°C at 5.185±0.005

bar (Angus et al., 1976), respectively. The P-T phase diagram is illustrated in Figure 1, the data is cited from Span and Wagner, 1996.

The saturation curve or vapour-liquid curve from the triple point to the critical point and melting curve can be written as the following Equations 1 and 2:

$$\log P_{sat} = \frac{-836.6}{T_{sat}} + 4.75 \quad (1)$$

$$P_{melt} = 523.18 - 51.547 * T_{melt} + 0.22695 * T_{melt}^2 \quad (2)$$

Where $P_{sat}$ and $P_{melt}$ are the vapour pressure in bar-a and $T_{sat}$ and $T_{melt}$ are the temperature in Kelvin.

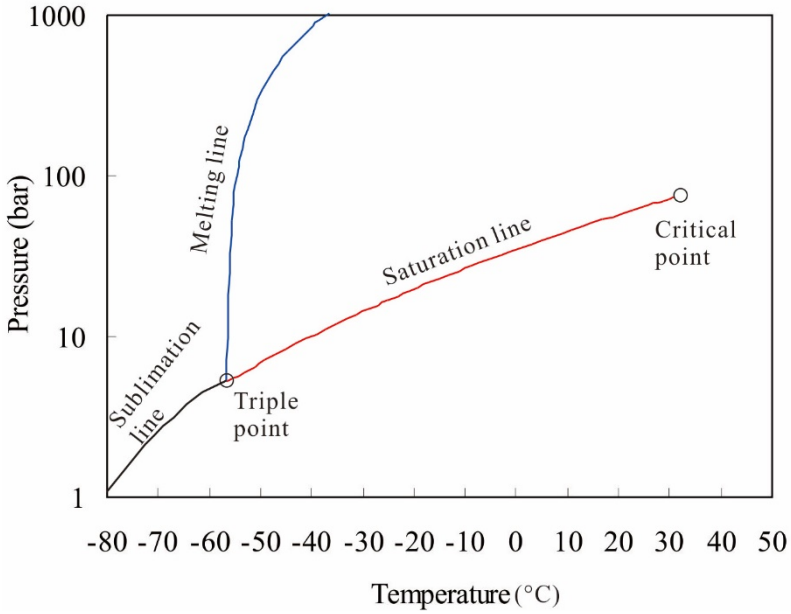


FIGURE 1: The P-T phase diagram of $CO_2$ (Data from Span and Wagner, 1996)

### 2.2 Equation of state for $CO_2$

The ideal gas law, introduced by Benoit Paule Emile in 1834, is the simplest equation of state (EOS) to describe how $CO_2$ behaves within different temperatures and pressures as shown by Equation 3.

$$P = \frac{nRT}{v} \quad (3)$$

Where $v$ is the molar volume; $n$ is the moles of gas and $R$ is the gas constant that is equal to 8.3145 $J \cdot mol^{-1} \cdot K^{-1}$. However, this equation is only satisfactory when the real gases are at relatively low pressures and temperatures. Later in 1873, J.D. van der Waals proposed a revised equation with two adjustable parameters (Equation 4) and it was modified by Kerrick and Jacobs in 1981 (Equation 5), which is consistent with experimental data of $CO_2$ and $H_2O$ at elevated temperatures and pressures.

$$P = \frac{RT}{v-b} - \frac{a}{v^2} \quad (4)$$

$$P = \frac{RT(1+y+y^2-y^3)}{v(1-y)^3} - \frac{a}{T^{0.5}v(v+b)} \quad (5)$$

Where $b$ is a constant and equal to 29.0 $cm^3 \cdot mol^{-1}$ and $a$ is a function of T and P, as follows:

$$y = \frac{b}{4v}$$

$$a(T,v) = c + \frac{d}{v} + \frac{e}{v^2}$$

$$c = (290.78 - 0.30276 \cdot T + 0.0014774 \cdot T^2) * 10^6\ bar \cdot cm^2 \cdot K^{0.5} \cdot mol^{-2}$$

$$d = (-8374 + 19.437 \cdot T - 0.008148 \cdot T^2) * 10^6\ bar \cdot cm^3 \cdot K^{0.5} \cdot mol^{-3}$$

$$e = (76600 - 133.9 \cdot T + 0.1071 \cdot T^2) * 10^6\ bar \cdot cm^4 \cdot K^{0.5} \cdot mol^{-4}$$

### 2.3 Chemical properties and carbon species

The $CO_2$ is an acidic and soluble gas and once it dissolves in water, carbonic acid will form and dissociate according to reactions listed in Equations 6-9. The equilibrium between $CO_2$ and $H_2O$ is determined by pH, temperature, pressure and salinity. Generally, the pH of the fluid controls the distribution of carbonate species and at low pH, aqueous $CO_2$ dominates ($H_2CO_3$) while at higher pH, bicarbonate and carbonic ions ($HCO_3^-$, $CO_3^{2-}$) are the dominant ions and a pH increase is likely to cause calcite scaling.

$$CO_{2(g)} \leftrightarrow CO_{2(aq)} \quad (6)$$

$$CO_{2(aq)} + H_2O \leftrightarrow H_2CO_3 \quad (7)$$

$$H_2CO_3 \leftrightarrow H^+ + HCO_3^- \quad (8)$$

$$HCO_3^- \leftrightarrow H^+ + CO_3^{2-} \quad (9)$$

The $CO_2$ solubility minimum is when the water temperature is at about 150°C-180°C (Figure 2), according to Henry's law and if there are also less soluble gases dissolved in the water, they will decrease the solubility of $CO_2$. Therefore, $CO_2$ degassing will be the most effective if boiling happens at this temperature range, leading to the greatest calcite super-saturation and scaling (Arnórsson, 1989).

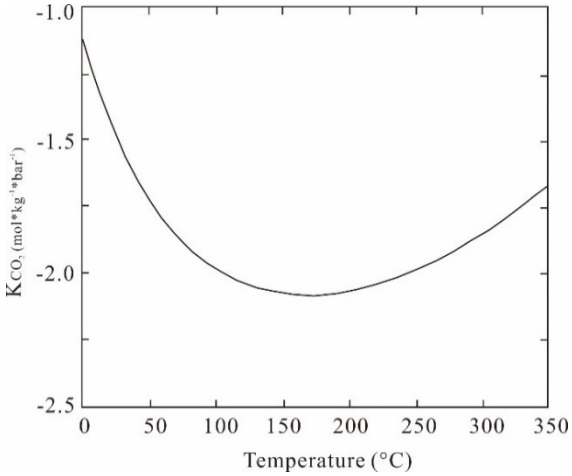


FIGURE 2: The $CO_2$ solubility in water, $K_{CO2}$ represents the Henry 'Law coefficient for $CO_2$ (from Arnórsson, 1989)

## 3. CALCITE SCALING IN THE GEOTHERMAL SYSTEM

### 3.1 Solubility of calcite

There are three polymorphs of calcium carbonate minerals in nature, calcite, aragonite and vaterite, and calcite is the most common carbonate mineral observed in the geothermal system. It is a secondary mineral and evidence from geothermal fluids with neutral to alkaline pH show that fluids at all temperatures are often saturated with respect to calcite (Bénézeth et al., 2013). The solubility of calcite at low temperatures (<100 °C) has been widely studied but most often the log K at 0°C to 90°C is taken from Plummer and Busenberg (1982) (Equation 10). For higher temperatures and more complex solutions, experimental data are scarce except that from Ellis (1963) and Segnit et al., (1962) at temperature range of 75°C - 201°C. In addition, a formula proposed by Arnórsson et al. in 1982 (Equation 11) is also widely used at temperatures up to almost 240°C (Arnórsson et al., 1982). Additional experimental data and models up to 60 bar $p_{CO2}$ and 300°C can precisely predict calcite solubility (Bychkov et al. in 2007, personal communication in Bénézeth et al., 2013).

$$\log K_{calcite} = -171.9065 - 0.077993 * T + \frac{2839.319}{T} + 71.595 * \log T \quad (10)$$

$$\log K_{calcite} = 10.22 - 0.0349 * T - \frac{2476}{T} \quad (11)$$

Calcite solubility measurements from 5°C to 300°C are summarized in Figure 3. The figure shows that predictions from Plummer and Busenberg (1982) and Arnórsson et al. (1982) are consistent at low temperatures of less than 90°C but both of them are slightly negative compared with experimental data from Jacobson and Langmuir (1974), Sass et al. (1983), Ellis (1963), Berner (1976), Gledhill and Morse (2006) and Bychkov et al. (2007). In the following calculations, calcite solubility functions from both Arnórsson et al. (1982) and a regression formula (Equation 12) based on all the collected data showed in Figure 3 are used.

$$\log K_{calcite} = -0.0001 * T^2 + 0.0092 * T - 8.5907 \quad (12)$$

In addition, calcite solubility under different $CO_2$ partial pressures and salinities (as NaCl) have also been studied as shown in Figure 4 (Nicholson, 1993). It is observed that calcite solubility increases with increasing $CO_2$ partial pressure but decreases with increasing temperature. Therefore, calcite scaling is the most intense where boiling is occurring. Cooling after boiling will later lead to a decrease of calcite saturation due to the retrograde solubility of carbonate minerals. From Figure 4(b), the calcite solubility increases with the increasing salinity of the fluid.

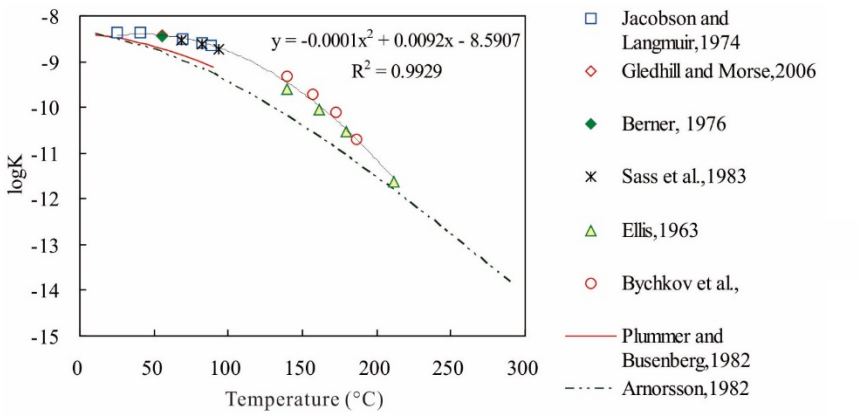


FIGURE 3: Calcite solubility as a function of temperature revised from Bénézeth et al. (2013), Jacobson and Langmuir (1974), Plummer and Busenberg (1982): 0°C - 90°C; Arnórsson et al., (1982): 0°C - 300°C; Sass et al. (1983): 0°C - 50°C; Ellis (1963): 98°C - 201°C; Bychkov et al. (personal communication from Bénézeth et al. (2013): 100°C -200°C

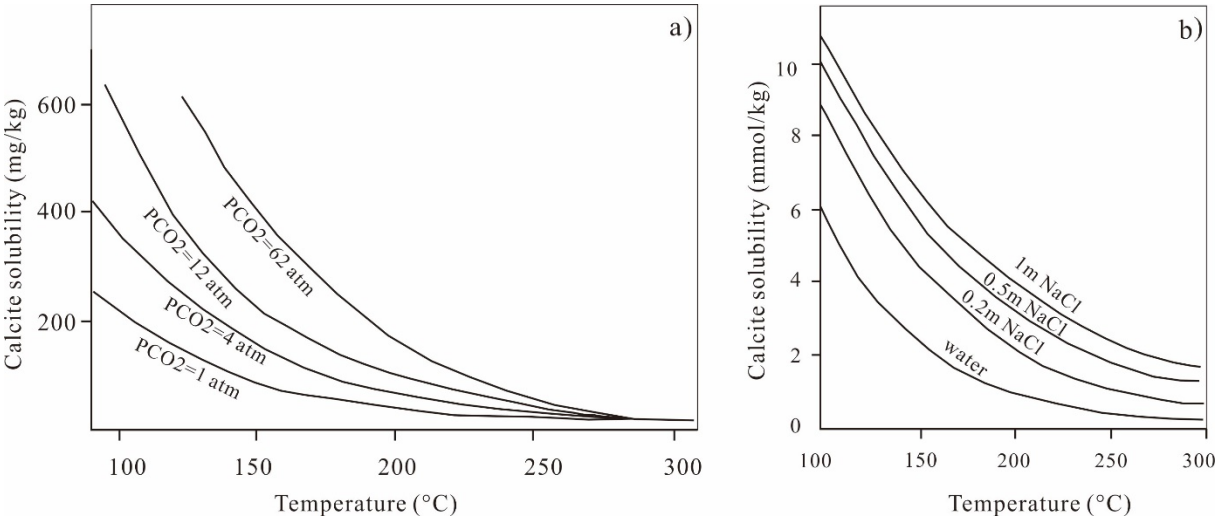


FIGURE 4: a) Calcite solubility as a function of temperature and different $CO_2$ pressures; b) Calcite solubility as a function of NaCl concentration under $P_{CO2}$=12 atm

### 3.2 Reasons for calcite scaling in geothermal systems

#### 3.2.1 pH increase due to boiling in the well

It has been concluded that calcite precipitation always occurs at the first level of boiling in the well (Arnórsson, 1989). When more $CO_2$ partitions to the steam phase (Equation 6 moves to the left) and the pH of the fluid is controlled by carbonic acid, the pH will increase and subsequently the concentration of carbonate ions ($CO_3^{2-}$) increases, causing the activity products of $Ca^{2+}$ and $CO_3^{2-}$ to increase and the fluid is more likely to be supersaturated with calcite which can precipitate as shown in Equation 13.

$$Ca^{2+} + CO_3^{2-} \rightarrow CaCO_3 \quad (13)$$

The rate and degree of precipitation increases with increasing super-saturation and water salinity. Pressure decline in the borehole will lead to a downward movement of the first boiling level, lengthening the scaling interval and the time for clogging the well. In practice, this process is often used as a mitigation method for calcite scaling (Arnórsson, 1978). For low temperature geothermal systems, the steam/water ratio is relatively low and the reaction rates and degassing extents are also limited, resulting in annular flow and impeding degassing. Therefore, generally, calcite scaling is not as serious as that in high temperature geothermal fields.

### 3.2.2 pH increase due to casing corrosion (Wanner et al., 2017)

Casing corrosion in the well will increase the pH of the fluid due to a consumption of protons ($H^+$) as shown in Equation 14.

$$\mathrm{Fe}^0_{(s)} + 2H^+ \rightarrow Fe^{2+} + H_2 \tag{14}$$

Typical corrosion products of Fe-bearing minerals in scales are not so common and the corrosion always occurs only at the interface of the uncoated casing. Once the casing is covered with scales, the corrosion will carry on at a rather slow rate because of protection from insolation. Therefore, pH increase from casing corrosion won't be a key factor for scaling during geothermal fluid production.

### 3.2.3 pH increase due to linear depressurization

Though pressure and minor temperature variations have little effect on calcite solubility, depressurization of the fluid does cause significant calcite super-saturation during the upwelling process. Calculations indicate that the increase of the calcite saturation index (CSI) due to depressurization can be ignored. The maximum CSI computed from wellhead samples and the concentration of dissolved inorganic carbon decrease due to calcite precipitation only account for 13 mol% (numerically calculated) (Wanner et al., 2017). Therefore, pH increase due to linear depressurization is also not the main drive of calcite scaling.

## 3.3 Calcite scale quantity assessment methods

### 3.3.1 Calcite scaling thickness (CST) assessment

The growth rate of calcite crystal surfaces during geothermal fluid production can be calculated using Equations 15 and 16 based on experiments on the kinetics of calcite scaling using a 1 mol NaCl solution with a temperature of 70°C, 90°C and a pH of 5.9 - 7.5 (Zhang and Dawe, 1998; Zhang et al., 2001).

$$R_L = K_p * (S^{0.5} - 1)^2 \tag{15}$$

$$\log K_p = 0.126 * (I)^{0.5} - \frac{2400}{T_k} - 2.11 \tag{16}$$

$$\log K_p = 0.126 * (I)^{0.5} - \frac{2400}{T_k} - 0.34 * pH + 0.444 \tag{17}$$

$$\log K_p = 0.126 * (I)^{0.5} - \frac{2400}{T_k} - 0.34 * pH + 0.222 \tag{18}$$

Where $R_L$ represents the linear growth rate of calcite crystal surfaces (m/s), S is the saturation ratio, which is equal to $10^{SI}$, $K_p$ is the empirical rate constant (m/s), $I$ is the ion strength (mol/kgw) and $T_k$ is the temperature in Kelvin (K).

Experimental results also showed that the calcite scaling rate is strongly affected by the pH and the lower the pH, the higher the growth rate. The influence of pH can be expressed by Equation 17 (Zhang et al., 2001). Also, Mg content in the fluid can inhibit calcite growth and if the Mg/Ca molar ratio is 0.1-

0.5, the calcite growth rate can be reduced by 40% (Dawe and Zhang, 1997). Formula 18 can be used for the calcite growth rate in solutions containing low concentrations of Mg. In addition, when the flow rate is higher than 0.5 m/s, $K_p$ will stabilize and become independent as indicated by experiments (Zhang and Farquhar, 2001). Then, the CST is calculated by multiplying $R_L$ and a constant time (e.g., 2 days expressed in seconds). From Equations 15, 16, 17 and 18, the CST depends on the temperature, ion strength, pH, saturation state of the fluid and the production time. Because the geothermal reservoir fluid is always in partial or full equilibrium with some minerals, including calcite, the method is therefore not suitable for reconstructed data. However, by assuming that the over-saturation extent and pH are constant (i.e., after $CO_2$ degassing started but before calcite nucleation), the CST can be derived and plotted as a function of temperature (Wolff-Boenisch and Evans, 2013). Though the experimental conditions do not cover the wide temperature and pH range that is typical for high-temperature geothermal systems (temperature higher than 150°C and pH between 7-9), the equations can still be used because the calcite scaling mechanism is the same for both low and high temperature fluids.

### 3.3.2 Calculation based on calcium content variations from bottom to wellhead

Ármannsson (1989) states that the difference in the calcium concentration along with data on flow and flow time for water samples collected at deep reservoirs and wellheads can be used to estimate the quantity of calcite depositions (Ármannsson, 1989). The formula is illustrated as Equation 19.

$$m_{caco3} = 2.5 * \Delta C_{ca} * v * t * 10^{-6} \quad (19)$$

Where $m_{caco3}$ is the total quantity of calcite deposits in kg; $\Delta C_{ca}$ is the difference of calcium concentration for water in the deep reservoir and at the wellhead in mg/kg; $v$ represents the flow rate of fluid from the well in kg/s; $t$ is the production time in seconds.

Data analysis from well KJ-9 showed that the quantity was about 2400 kg which was almost consistent with the measurement using a calliper log (2700 kg). Therefore, his method can be tried for calcite scale estimation.

### 3.3.3 Calculation based on WATCH and PHREEQC simulations

It is better to obtain deep fluid samples, especially before flashing, to compute in the PHREEQC programme. However, sometimes a representative reservoir sample can't be obtained due to various reasons and therefore, the WATCH program can be used to reconstruct the compositions of the deep fluid using wellhead discharge water and steam data. Then we can use the reservoir fluid chemical compositions as the input for the PHREEQC programme. WATCH assumes a mass balance, however calcite precipitation during boiling may decrease the calcium content to some degree. The possible calcite precipitation amounts (mmol/kgw) are calculated by assuming the calcite saturation index to be 0 in the Equilibrium-Phase keyword in PHREEQC. The total scale quantity can be assessed by Equation 20.

$$m_{caco3} = 100 * \Delta m_{caco3} * v * t * 10^{-6} \quad (20)$$

Where $m_{caco3}$, $v$ and $t$ have the same meaning as for Equation 19 and $\Delta m_{caco3}$ represents the maximum calcite precipitation amount per kg water.

## 4. STUDY AREA

### 4.1 Site location and geological setting

The Kangding geothermal field is located in the western Sichuan plateau with an average elevation of more than 3000 m a.s.l. (Figure 5) and it is also known as the east syntax formed due to the collision of

the Indian Plate and the Eurasian Plate. The mean annual temperature and precipitation are about 7.1°C and 832 mm, respectively, according to historical meteorological records. Studies of fault systems indicate that large-scale strike-slip faults are widely developed with orientations of NWW and NNE and they are active, as evidenced from seismic activities occurring in recent years, (e.g. Wenchuan, Ya'an and Jiuzaigou seismic activities, Xu et al. 2011). There are three significant faults in the study area, namely the Longmenshan fault, Xianshuihe fault and Anninghe fault, which form a Y shape (Figure 5). Along the Xianshuihe fault, intrusive rocks with different ages were investigated: 1) in the east, the oldest group is formed of monzonitic granite and plagiogranite, 2) in the central part there is a group which is 110 Ma - 210 Ma old, and 3) in the south, the youngest batholith is found with an age of 13 Ma -10 Ma (Xu and Kamp, 2000).

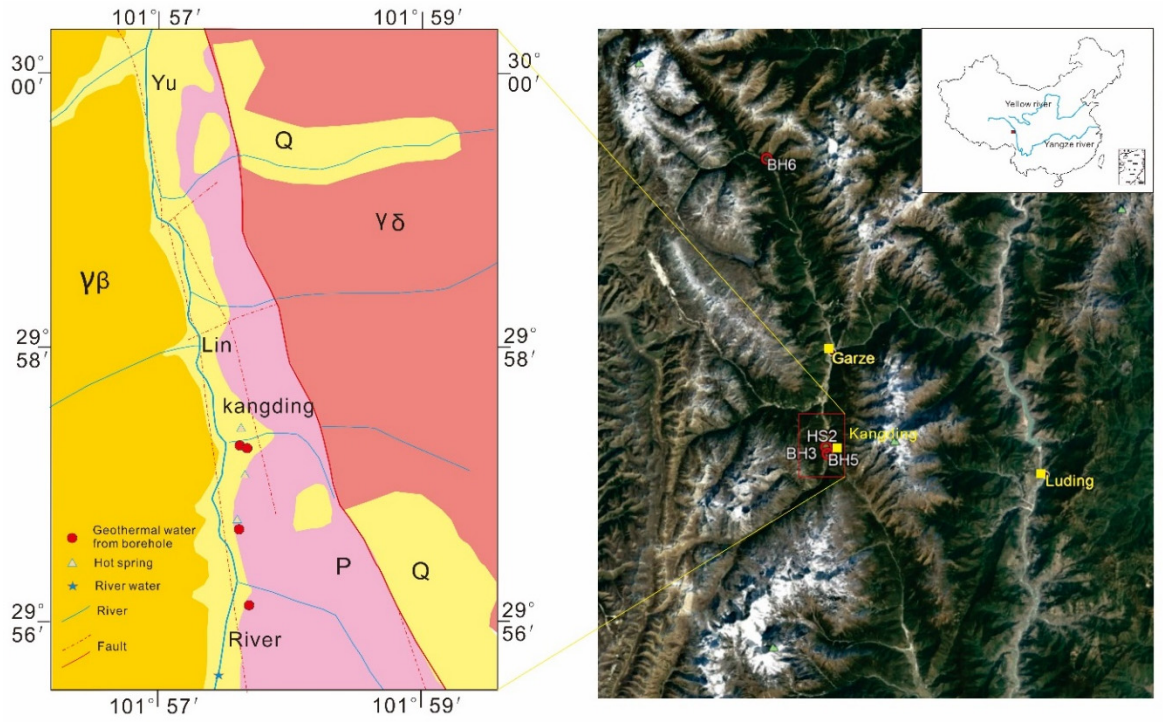


FIGURE 5: Site location and basic geological conditions

The exposed strata in the area are mainly composed of unconsolidated sediments, sedimentary rocks (slate and quartz schist), and metamorphic rocks (crystalline limestone, marble and phyllite) dated from the Quaternary to the Permian without the Mesozoic. Well drilling of BH6 reveals that from depth of about 100 m to 1847 m, the lithology shows sedimentary rocks of slate and quartz schist (Long, 2014).

Previous work shows that the heat flow value in west Sichuan is 76 ±12.8 mW/m$^2$ while the newest measurements indicate a higher geothermal background with values as high as 94.7 mW/m$^2$ in the Aba area, north of Kangding (Hu et al., 2001; Jiang et al., 2016). In addition, strong surface manifestations have been observed in this area, including hydrothermal explosions, hot springs, fumaroles and sinters. Hot springs with temperatures of 21°C - 87.5°C and discharges of 0.1 l/s - 10 l/s as well as 24 exploration wells with measured downhole temperatures up to 209°C, have been investigated (Tong and Zhang, 1994; Guo et al., 2017).

## 4.2 Geothermal system descriptions

### 4.2.1 Fluid geochemistry of Kangding geothermal field

Based on geochemical data (Table 1), there are three types of water, namely deep geothermal fluids from boreholes, shallow geothermal water from shallow boreholes and hot springs and river water. The

deep geothermal fluid (BH1, BH2, and BH3) has high pH ranging from 7.3 to 9.5 with wellhead temperatures of 104°C-178°C. It is of a $HCO_3$·Cl-Na type (Figure 6) and the total dissolved solids (TDS) are 2323 -2553 mg/L. The temperature of the shallow geothermal fluid is 47.5°C- 82°C which is much lower compared to the deep fluid, and belongs to the $HCO_3$·Cl-Na and $HCO_3$-Na·Ca types based on chemical composition (Figure 6). The TDS of the shallow geothermal fluid (802 -2168 mg/L) is lower than that of the deep fluid. The river water collected from the Yulin river represents the cold water end-member if mixing occurs. Its TDS is low and it equals to 83 mg/L. It also belongs to the $HCO_3$·$SO_4$-Ca·Mg type. Evidence from water isotopes indicate that the geothermal fluid is recharged by snowmelt and local precipitation and its chemical composition results from the mixing between meteoric and magmatic waters (Guo et al., 2017).

TABLE 1: The chemical composition of geothermal water from boreholes, hot springs and river (mg/L)[1]

| Sample ID | BH1 | BH2 | BH3 | BH4 | BH5 | BH6 | HS1 | HS2 | HS3 | RW |
|---|---|---|---|---|---|---|---|---|---|---|
| Original ID | 15J35 | 15J36 | 15J38 | 15J42 | 15J37 | DKZ02 | 15J39 | 15J41 | 15J43 | 15J40 |
| Discharge type | Geothermal water from boreholes | | | | | | Hot springs | | | River water |
| Well depth (m) | 656 | 267 | 305 | 109 | 248 | 1847 | | | | |
| pH | 9.5 | 9.1 | 8.5 | 9.0 | 7.3 | 7.8 | 7.5 | 7.7 | 6.7 | 8.2 |
| T(°C) | 178 | 150 | 104 | 118 | 82 | 115 | 47.7 | 81 | 47.5 | 6.2 |
| TDS | 2323 | 2359 | 2350 | 2553 | 2168 | 2379 | 1661 | 1066 | 802 | 83.0 |
| B | 2.0 | 1.9 | 1.8 | 2.2 | 1.4 | 2.2 | 1.1 | 0.6 | 0.3 | 0 |
| Na | 670 | 686 | 673 | 727 | 617 | 570 | 426 | 246 | 117 | 2.4 |
| K | 142 | 122 | 120 | 124 | 102 | 50.0 | 68.6 | 41.1 | 18.9 | 0.9 |
| Ca | 3.5 | 2.2 | 3.2 | 1.9 | 38.9 | 22.0 | 73 | 49.1 | 119 | 19.2 |
| Mg | 0.2 | 0 | 0.3 | 0.2 | 5.5 | 6.1 | 14.7 | 14.9 | 18.1 | 4.6 |
| Al | 0.6 | 0.7 | 0.1 | 0.2 | 0.1 | 0 | 0 | 0 | 0 | 0 |
| Cl | 678 | 655 | 750 | 738 | 602 | 144 | 396 | 193 | 73.3 | 2.4 |
| $SO_4$ | 23.0 | 27.0 | 6.0 | 14.4 | 0 | 15.8 | 3.7 | 68.3 | 53.1 | 16.9 |
| F | 6.9 | 7.8 | 5.0 | 7.7 | 2.9 | 7.9 | 3.1 | 1.6 | 1.2 | 0.4 |
| $HCO_3$ | 542 | 787 | 1018 | 950 | 1259 | 1428 | 1059 | 618 | 636 | 58.8 |
| $CO_3$ | 324 | 227 | 51.8 | 176 | 0 | 0 | 0 | 0 | 0 | 0 |
| $SiO_2$ | 355 | 341 | 247 | 367 | 162 | 136 | 140 | 141 | 82.5 | 6.4 |

1. All the data taken from Guo et al., 2017, except BH6 which is from Wang et al., 2015.

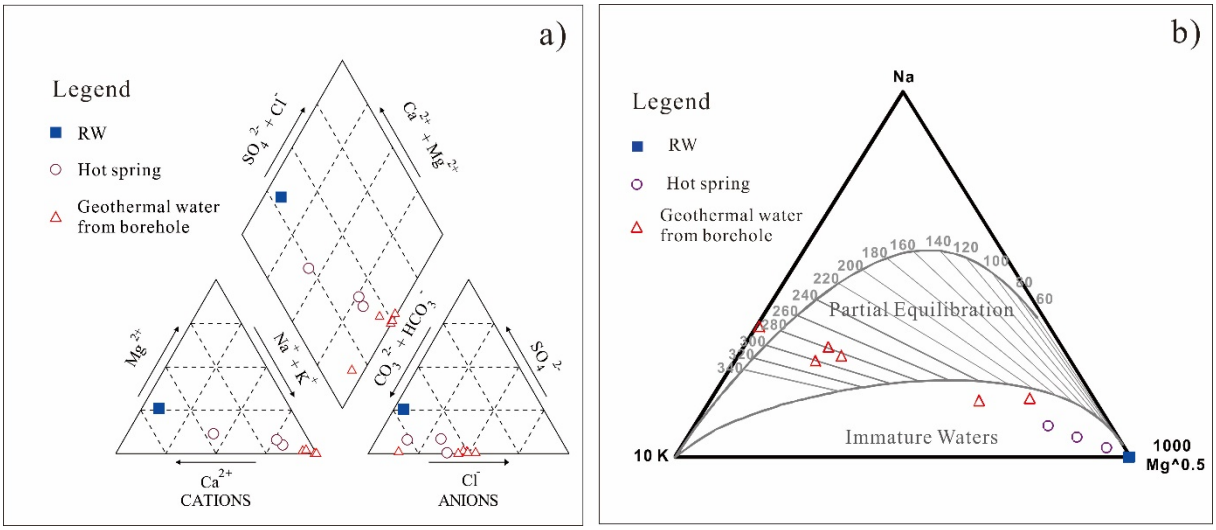


FIGURE 6: Piper diagram for various water from Kangding geothermal fields

### 4.2.2 Scaling problems

Serious scaling occurred during a 48 hour discharge test of well BH6 and 1-3 cm thick scale was observed in the surface pipe as shown in Figure 7 (Zhang et al., 2016). Results from XRD and XRF analysis show that the scale is mainly composed of $CaCO_3$ (> 95% by weight) and traces of amorphous $SiO_2$ (Wang et al., 2015). Due to the calcite scaling problem, this well is still not in production.

FIGURE 7: Calcite scales in the pipeline (left) and flange (right)

## 5. DATA SOURCES AND ANALYTICAL METHODS

### 5.1 Data sources

The river water, borehole geothermal water and hot spring chemical compositions have been previously described (Wang et al., 2015; Guo et al., 2017). A total of ten samples were collected in August 2013 and October 2015, as shown in Figure 5. The borehole depth ranges from 109 m to 1847 m and all the geothermal samples were collected at the wellhead using a simple water-vapour separator. Water temperature, electrical conductivity (EC), pH and oxidation reduction potential (ORP) were measured onsite using a portable multiparameter (HQ40D, Hach). Bicarbonate and carbonate ions were also measured onsite using a digital titrator (Model 16900, Hach) with 0.8 N $H_2SO_4$ with bro-mocresol green-methyl red as indicator. All the samples, except the $SiO_2$ samples, were filtered through a 0.23 μm membrane and sealed with parafilm to avoid evaporation. Cations and trace element samples were acidified to pH < 2.0 with 6 N super pure $HNO_3$ for preservation before analysis. Filtered but un-treated samples were stored in HDPE bottles for anion analysis. Samples collected for $SiO_2$ analysis were diluted on site using deionized water. For water isotope analysis, raw samples were collected and refrigerated before analysis. Two gas samples from the separator at the wellhead were also collected using a drainage gas-collecting method.

The contents of cations and trace elements were determined by ICP-AES (ICAP6000) and ICP-MS (7500C, Agilent), respectively, while anions were analysed with Ion Chromatography (Dionex ICS600) in Chinese University of Geosciences (Beijing). Precision for cations and anions are reported to be less than 0.5%. Water isotopes ($\delta^{18}O$, $\delta^{2}H$) were detected by a laser absorption water isotope spectrometer analyser (L1102-I, Picarro) at the Institute of Geology and Geophysics, Chinese Academy of Sciences. The precisions of $\delta^{18}O$ and $\delta^{2}H$ are 0.1‰ and 0.5‰ VSMOW respectively.

### 5.2 Data interpretations by modelling

For better interpretation of the geochemical data and investigation of the deep reservoir chemical composition, the WATCH and PHREEQC computer codes are used. For the calcite scaling depth assessment, the HOLA and WELLSIM computer codes are used.

#### 5.2.1 The WATCH computer code

The WATCH was originally written in the 1970s by Stefán Arnórsson, Sven Sigurðsson, and Hörður Svavarson. In 1993, it was rewritten and later on updated by Jón Örn Bjarnason (1994). The present 2.4 version updated in 2010 is written in FORTRAN 77 though it does not follow the ANSI standard strictly. References for the WATCH thermodynamic database can be found in Arnórsson et al., (1982).

The programme includes mass balance equations of species and mass action equations of chemical equilibria between species. These two sets of equations are solved simultaneously by an iterative procedure which is carried out a few times during each run of the programme. The programme contains provisions for 67 different aqueous species in total, in addition to $H^+$ and $OH^-$.

Generally, the results of a chemical analysis of water, gas and steam condensate samples are used to reconstruct the chemical compositions of downhole or deep fluids, including pH, aqueous speciation, partial pressures of gases, redox potentials, and activity products of minerals. In addition, the programme can also be used to compute the resulting species concentrations, activity coefficients, activity products and solubility products when adiabatically boiled or conductively cooled from the reference temperature to some lower temperature. This is particularly useful in the study of scaling (Iceland Water Chemistry Group, 2010).

#### 5.2.2 The PHREEQC computer code (Parkhust and Appelo, 1999)

The PHREEQC program is developed by David L. Parkhust and C.A.J. Appelo from the United States Geological Survey (USGS). The present version 3 is written in the C and C++ programming language and is designed to perform a wide variety of low-temperature aqueous geochemical calculations. It implements several types of aqueous models: two ion-association aqueous models (the Lawrence Livermore National Laboratory model and WATEQ4F), a Pitzer specific-ion-interaction aqueous model, and the SIT (Specific ion Interaction Theory) aqueous model. Using these aqueous models, PHREEQC has capabilities for (1) speciation and saturation-index calculations; (2) batch-reaction and one-dimensional (1D) transport calculations with reversible and irreversible reactions, which include aqueous, mineral, gas, solid-solution, surface-complexation, and ion-exchange equilibria, and specified mole transfers of reactants, kinetically controlled reactions, mixing of solutions, and pressure and temperature changes; and (3) inverse modelling, which finds sets of mineral and gas mole transfers that account for differences in composition between waters within specified compositional uncertainty limits.

All input for PHREEQC version 3 is defined in keyword data blocks, each of which may have a series of identifiers for specific types of data.

#### 5.2.3 The HOLA computer code (Björnsson, 1987)

The HOLA code is a wellbore simulator and was developed by Grimur Björnsson in 1987 using FORTRAN. It enables the computation of downhole conditions in wells with an arbitrary number of feed zones during discharge or injection. Calculations can be either at the well-head and continue downwards in a finite difference grid or from the bottom and proceed upwards. Two phase mixtures are assumed to flow upwards while single-phase fluid can flow either up or down.

The code has many potential applications: (1) designing multi-feedzone wells; (2) matching flowing temperature and pressure profiles to determine flow rates and enthalpies of individual feed zones; (3) studying flow in the well and optimizing the operating wellhead conditions to maximize productivity; (4) studying multiple feed zones using pressure transient data during well tests; (5) coupling with a reservoir simulation to determine well productivity or infectivity changes with time; (6) flashing depth calculation.

Generally, computations are done in two steps: (1) balance is given to the wellbore and feedzone mass and energy fluxes at the grid node where the feedzone is encountered to find the inlet conditions for the next unknown section of the well; (2) calculate the flow conditions in the well between feedzones. These two steps are repeated until the program reaches the other end of the grid.

### 5.2.4 The WELLSIM code (Gunn and Freeston, 1991; GSDS, 2017)

The WELLSIM is an integrated geothermal wellbore simulator and analysis package designed to allow 'what-if' scenarios to be performed on a geothermal well. It was written by Gunn and Freeston in 1991 and now it has been updated by the Geothermal Science and Data Solution (GSDS). It includes five modules: discharge test simulation, fluid composition and properties calculation, deliverability curve prediction, statistical and graphical matching analysis of downhole pressure and temperatures, and downhole measurement analysis.

Theoretical equations including the conservation of mass, the conservation of energy and the conservation of momentum are used to govern the single phase flow while empirical equations developed by the engineers are used to deal with two-phase flow, such as flow correlation and equation of state.

## 6. RESULTS AND DISCUSSION

### 6.1 Reservoir fluid compositions reconstruction

For borehole samples in Kangding geothermal field, the WATCH boiling spring model was applied to reconstruct deep fluid compositions. This model has been used due to a lack of steam data caused by sampling problems. From the Giggenbach Na-K-Mg diagram (Guo et al., 2016), BH1, BH2, BH3 and BH4 samples were in fully or partial equilibrium, therefore, it is assumed that mixing had little effect on these four samples and the calculated WATCH Na-K geothermometer was used as reference temperature. The reconstructed deep fluid chemical compositions from four borehole samples are listed in Table 2. Results showed that the reservoir temperature is about 260°C-280°C and the original pH ranges from 6.2 to 7.7. The fluid is of $HCO_3$·Cl-Na and Cl·$HCO_3$-Na types and there are substantial amounts of aqueous $CO_2$ in the fluid which may be the carbon source of the potential calcite scale.

TABLE 2: Calculated deep fluid chemical compositions from borehole samples using WATCH

| Sample No. | Ref. T (°C) | pH | $CO_2$ | B | $SiO_2$ | Na | K | Mg | Ca | F | Cl | $SO_4$ | Al |
|---|---|---|---|---|---|---|---|---|---|---|---|---|---|
| BH1 | 283 | 7.66 | 2208 | 1.50 | 267 | 504 | 107 | 0.15 | 2.63 | 5.19 | 510 | 17.30 | 0.45 |
| BH2 | 263 | 6.99 | 4958 | 1.43 | 257 | 518 | 92.03 | 0.04 | 1.66 | 5.88 | 494 | 20.37 | 0.53 |
| BH3 | 265 | 6.23 | 22718 | 1.22 | 167 | 456 | 81.47 | 0.20 | 2.17 | 3.39 | 508 | 4.07 | 0.07 |
| BH4 | 259 | 6.66 | 8434 | 1.57 | 262 | 518 | 88.08 | 0.14 | 1.35 | 5.49 | 526 | 10.26 | 0.14 |

The BH5 wellhead temperature was 82°C and the local boiling temperature was about 90°C at an altitude of 3100 m and it is assumed that mixing happened. Therefore, for hot spring samples and the BH5 borehole sample, the silica-enthalpy model was used to calculate the mixing ratio (Truesdell and Fourier,

1977) and reconstruct the deep fluid. It has been shown that the hot springs resulted from mixing between deep fluid and shallow cold water (Guo et al., 2016). The silica-enthalpy plot for these hot spring samples and BH5 is shown in Figure 8.

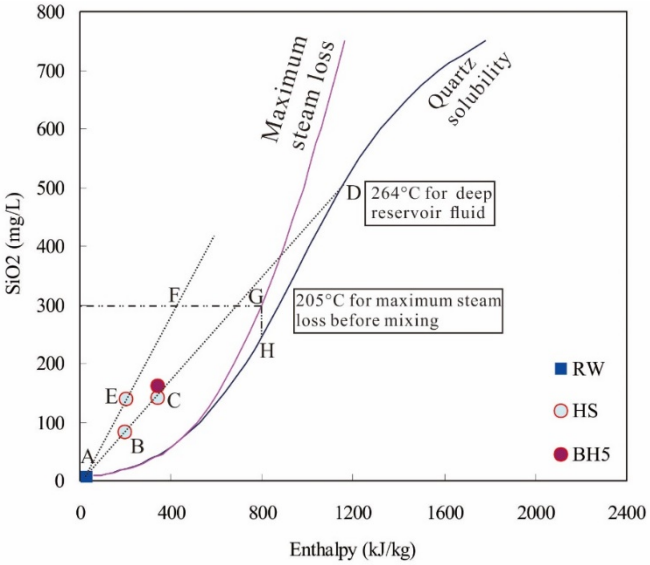


FIGURE 8: The Silica-enthalpy model for hot spring samples and BH5 in Kangding geothermal field

The RW sample represents the cold water end-member because it was collected in the local Yulin River that is recharged by meteoric waters. Point D represents the enthalpy and silica content of the deep fluid for samples HS2, HS3 and BH5. The fraction of deep hot water for the hot springs can be determined by dividing the distance AB by AD or AC by AD. The results indicate that the mixing ratio of deep fluid for HS3 and BH5 is about 26.9% while that for HS2 is about 15.3% (Table 3). For HS1, it is assumed that steam loss from an adiabatically cooled liquid occurred before mixing with cold water, therefore, the fraction of deep hot water is obtained by dividing the distance of AE by AF. Besides, the weight fraction of the original reservoir fluid lost as steam before mixing can be calculated using Equation 21. Results indicated that for HS1, the fraction of hot water is about 45.4% and the weight fraction lost as steam is about 14%. Based on these mixing ratios, the deep fluid compositions from hot springs HS2 and HS3 were reconstructed (Table 4). From the mixing model, the deep reservoir fluid for HS2 and HS3 should be similar. However, the pH, Ca, Mg, and Cl substantially differ. The recalculated pH from HS3 using the mixing ratio is negative and this is probably because apart from mechanical mixing, no other geochemical reactions during the upwelling of HS3 were included.

$$x = 1 - \frac{silica\ content\ at\ point\ H}{silica\ content\ at\ point\ G} \tag{21}$$

TABLE 3: Fraction of deep fluid calculations using silica-enthalpy mixing model

| Sample No. | Type | T (°C) | $SiO_2$ (ppm) | Enthalpy (kJ/kg) | Fraction of deep fluid (%) | Weight fraction of original hot water lost as steam before mixing (%) |
|---|---|---|---|---|---|---|
| HS1 | Hot spring | 82.0 | 161.8 | 343.3 | 45.4 | 14 |
| HS2 | | 47.7 | 139.7 | 199.7 | 26.9 | |
| HS3 | | 81.0 | 140.5 | 339.1 | 15.3 | |
| BH5 | Shallow geothermal water | 47.5 | 82.5 | 198.9 | 26.9 | |
| RW | River water | 6.2 | 6.4 | 26.1 | | |
| D point | | | 505.0 | | | |
| C point | | | 140.5 | | | |
| B point | | | 82.5 | | | |
| G point | | | 300.0 | | | |
| H point | | | 258.0 | | | |

TABLE 4: Reconstructed deep fluid compositions from hot spring HS2 and HS3 (mg/L)

| Sample No. | T(°C) | pH | Li | B | Na | K | Ca | Mg | Cl | $SO_4$ | F | $HCO_3$ | $SiO_2$ |
|---|---|---|---|---|---|---|---|---|---|---|---|---|---|
| HS2-R | 283 | 6.3 | 10 | 2.2 | 904 | 150 | 130 | 42.7 | 708 | 207 | 4.8 | 2129 | 503 |
| HS3-R | 282 | -1.8 | 8 | 2.0 | 764 | 121 | 681 | 94.6 | 475 | 258 | 5.7 | 3908 | 514 |

The fluid chemical compositions for BH6 calculated using the boiling spring model of WATCH is not representative. The measured discharge Ca concentration used in the simulation doesn't include the Ca formed during calcite scale deposition which had been observed in the well (Figure 7). Therefore, the data obtained from the WATCH boiling calculations was used in the PHREEQC model to reconstruct the reservoir fluid compositions. It was assumed that the reservoir fluid is at equilibrium with calcite by forcing the saturation index of calcite to be 0.The computed BH6 chemical components from PHREEQC were again used in the WATCH simulation for further calculations and the results are shown in Table 5. The results of those calculations indicate that calcite scaling doesn't change the concentrations of Na, K, $SiO_2$, B, F, Cl and $SO_4$, but it decreases the Ca, Mg and $CO_2$ concentrations during scaling formation. Therefore, recalculations of the deep geothermal fluid where scaling occurs are required to ensure for those losses.

TABLE 5: Observed and calculated deep fluid chemical compositions for BH6

| Sample NO. | pH/ T (°C) | B | $SiO_2$ | Na | K | Mg | Ca | F | Cl | $SO_4$ | Al | Fe | $CO_2$ | $H_2S$ |
|---|---|---|---|---|---|---|---|---|---|---|---|---|---|---|
| | | mg/L | | | | | | | | | μg/L | | mg/L | |
| Wellhead | 7.80/25 | 2.2 | 136 | 570 | 50.0 | 6.1 | 22.0 | 7.9 | 144 | 15.8 | 2.0 | 20 | 1030 | 1.14 |
| Deep water (T=150°C)[1] | 5.59/150 | 2.1 | 127 | 532 | 46.7 | 5.7 | 20.6 | 7.4 | 134 | 14.8 | 1.9 | 19 | 10840 | 4.27 |
| Deep water (T=150°C)[2] | 5.63/150 | 2.1 | 128 | 539 | 47.1 | 5.7 | 44.8 | 7.5 | 136 | 15.2 | 1.9 | 20 | 7938 | 4.13 |

1. Calculated using the spring boiling model in WATCH 2.4 with the wellhead data;
2. Calculated using the PHREEQC program with reconstructed data from WATCH by assuming calcite equilibration in the deep water;

## 6.2 Calcite scaling potential assessment

### 6.2.1 General assessment for both borehole and hot spring samples

The calcite scaling potential for the Kangding geothermal field is assessed using the WATCH programme with data both from boreholes and hot springs. The activity product (log ($Ca^{2+}$) ($CO_3^{2-}$)) of calcite is calculated for wellhead temperatures and reference temperatures with respect to chalcedony, quartz and Na-K geothermometers as shown in Figure 9. The calcite saturation line (Arnórsson et al., 1982) and regression equation (Equation 12) are used to check fluid properties. Results show that most of the samples are over-saturated with respect to calcite, especially when referring to the calcite saturation line. It is worth noting that even at reservoir conditions (reconstructed fluid with chalcedony, quartz and Na-K geothermometers), the fluid is still over-saturated with respect to calcite in all the samples except BH6.

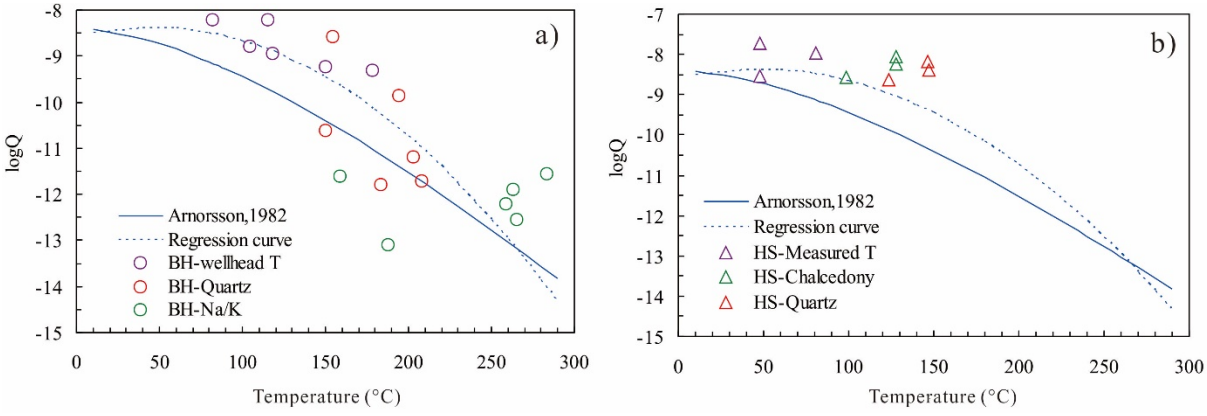


FIGURE 9: Calcite saturation state variations with temperature for borehole (a) and hot spring samples (b)

### 6.2.2 Analysis of BH6 sample

Serious calcite scaling had been observed in this well. Wellhead and bottom temperatures were measured to be 115°C and 145°C respectively. Although the temperature of this well is lower than 200°C, it has proved that quartz equilibrium is achieved and therefore, the WATCH quartz geothermometer was chosen to calculate the reference temperature. Data re-corrected using PHREEQC programme (deep water [2] in Table 5) were used in WATCH for the adiabatical boiling at 145°C, 135°C, 125°C and 115°C. Results from the spring boiling model calculation show that the steam fraction at the wellhead is 6.0% and the fluid is slightly under-saturated with respect to calcite (Figure 10). It becomes over-saturated during boiling at different temperatures which may result in scaling problems. The pressure decrease during boiling will cause the $CO_2$ loss (Figure 2). With the decreasing temperature during boiling, the fluid becomes saturated with respect to chalcedony and quartz (Figure 10). Amorphous silica is under-saturated during this process and therefore silica scaling is not likely to occur. Note also that quartz precipitation kinetics is slow in those conditions.

During the boiling process, substantial amounts of aqueous $CO_2$ move into the gas phase causing the pH to increase when the fluid pH is controlled by the carbon acid balance (Figure 11). With the pH increase, the carbonic ion ($CO_3^{2-}$) content increases and aqueous $CO_2$ decreases (Figure 11). The concentration of bicarbonate ions ($HCO_3^-$) decreases slightly. The

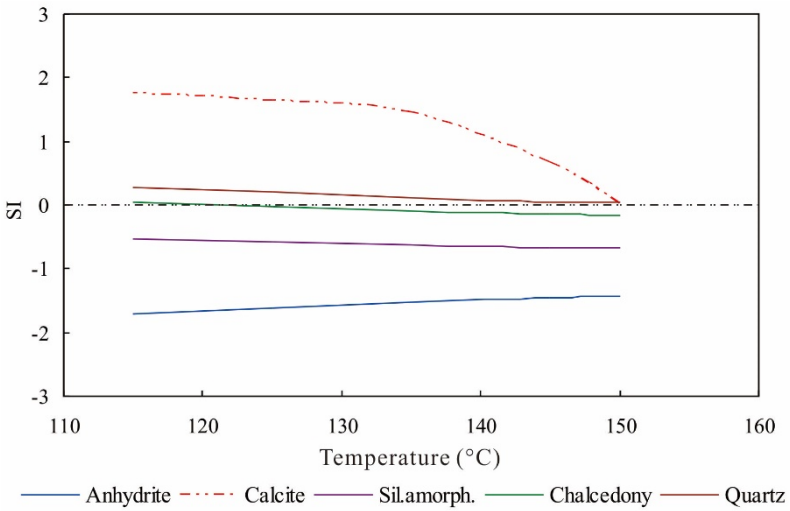


FIGURE 10: Mineral saturation state variations with temperature during boiling process

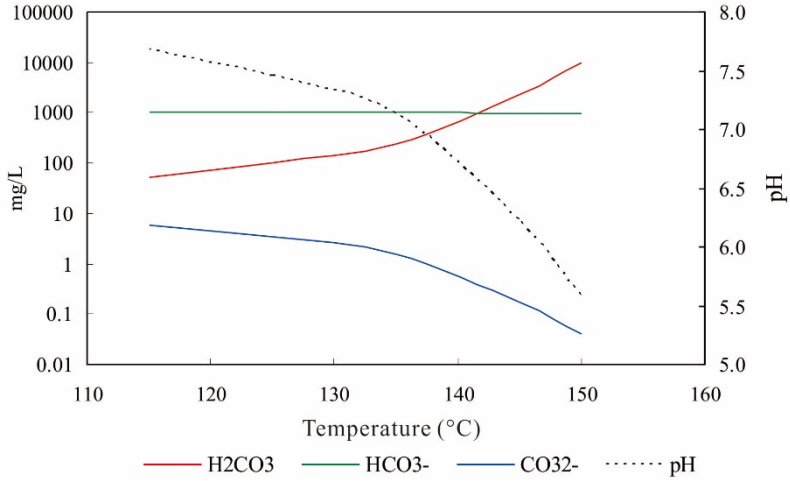


FIGURE 11: Carbon speciation and pH variation during boiling process

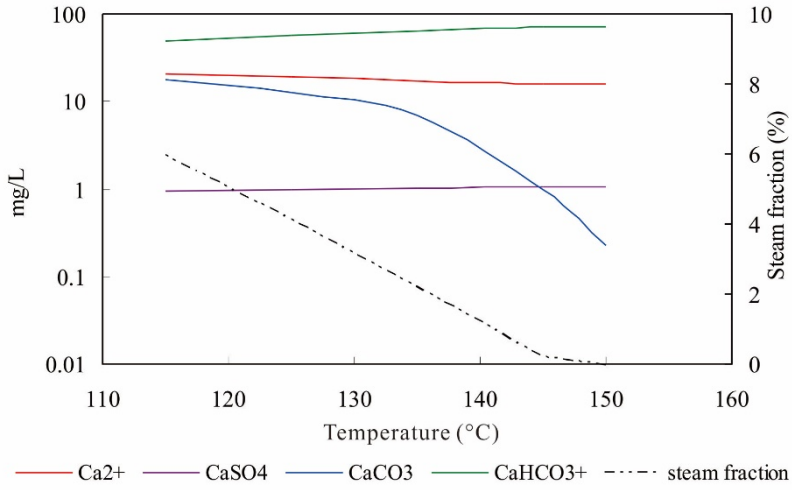


FIGURE 12: Calcium speciation and steam fraction variation during boiling process

chemical reaction for the second order of carbon acid dissociation moves to the left side (Equation 9) and subsequently, leads to an increase of the activity product of calcite ($CaCO_3$) and over-saturation of calcite (Figure 10). It is observed that the $CaCO_3$ content in the fluid increases from 0.2 mg/L to 17.8 mg/L after boiling, while the $CaHCO_3^+$ content decreases (Figure 12) due to carbonic acid balance changes due to boiling. This is also consistent with the calcite over-saturation in the fluid. The $Ca^{2+}$ concentration in the fluid shows a slightly increase from 15.7 mg/L in the reservoir to 20.5 mg/L at the wellhead which is probably caused by steam loss.

### 6.3 Scaling depth

The scaling depth is always several meters above the boiling depth (Akin et al., 2015). Results from wellbore modelling and PHREEQC calculations indicate that calcite is not over-saturated as soon as gas bubbles arise, but appears to precipitate 80 m after the boiling depth (Akin et al., 2015). Since scaling depth cannot be assessed directly, the boiling depth is calculated instead. The boiling depth is calculated with the HOLA and WELLSIM programmes. The basic equations for these two programmes are almost the same, except that WELLSIM takes into account $CO_2$ and salinity.

For the HOLA program, the input parameters are the wellhead parameters (wellhead pressure in bar-abs, wellhead enthalpy in kJ/kg, wellhead flow rate in kg/s), heat loss parameters (rock thermal conductivity in w/m/°C, rock density in kg/m$^3$), wellbore geometry and feedzone properties. The wellhead pressure and enthalpy for BH6 are assumed to be 1.9 bar-abs and 615 kJ/kg, respectively (Wang et al., 2015; Zhang et al., 2016). The possible scaling depth is calculated to be about 150 m (Appendix 1, Figure 13). The dryness (also called steam fraction) at the wellhead is about 5.3% which is comparable with that reconstructed with the boiling spring model (6.0%).

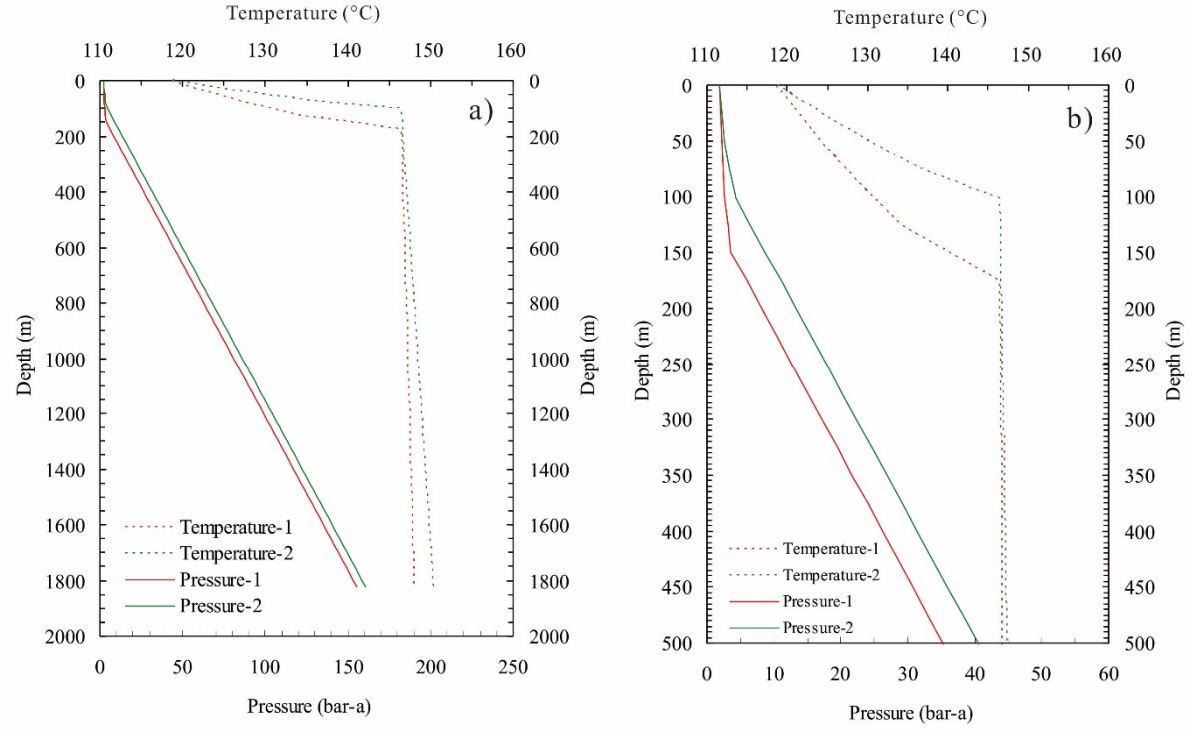


FIGURE 13: Boiling depth calculation using HOLA and WELLSIM, Temperature-1 and Pressure-1 are from HOLA; Temperature-2 and Pressure-2 are from WELLSIM without $CO_2$

For the WELLSIM programme, the input data includes the flow rate, wellbore geometry, feedzone properties (optional), fluid dryness, fluid impurities (e.g. $CO_2$ and NaCl in total fluid) and two of either

pressure, temperature or enthalpy. The discharge simulation will calculate the conditions in a well discharging at a given steady-state mass flow rate. Three $CO_2$ concentrations are used to run the programme, the first one is 0 ppm as in the HOLA; the second one is the $CO_2$ content at the well bottom where the temperature is about 145°C which is 2352 ppm, and the third one is based on the calculated $CO_2$ content in the deep water from PHREEQC which is 7938 ppm. Detailed results are shown in Appendices 2, 3 and 4. The simulation results indicate that no $CO_2$ is present (Figure 14) and the boiling depth is about 100 m. At a low $CO_2$ content (2352 ppm), the possible scaling depth is the same as that from the HOLA program or 175 m (Figure 14) with the dryness calculated to be 5.6%, consistent with that calculated from WATCH. At a high $CO_2$ concentration (7938 ppm), the fluid begins to boil at about 440 m and boiling continues to a depth of 250 m (Figure 14). The dryness is calculated to be about 6.2%.

As shown in Figure 14, the boiling depth is positively related to the $CO_2$ concentration so when the $CO_2$ content is higher, the boiling depth is deeper. This is because when $CO_2$ content is higher and boiling happens, more $CO_2$ goes to the gas phase and the gas pressure increases, causing the increase of boiling depth. This is also called pumping effect of $CO_2$.

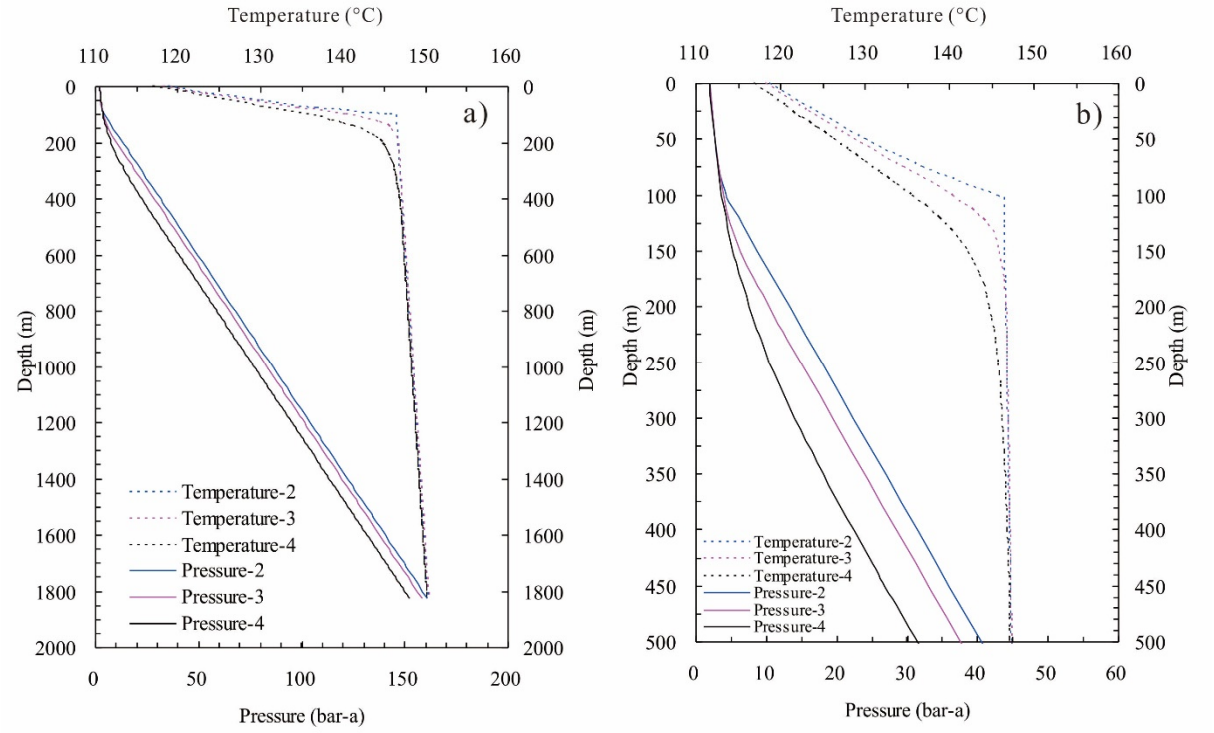


FIGURE 14: Boiling depth calculation using WELLSIM, Temperature-2, 3, 4 and Pressure-2, 3, 4 refer to $CO_2$ content in the fluid of 0, 2352 ppm and 7938 ppm, respectively

The friction and acceleration losses are small and the main cause of the pressure decrease with fluid upwelling to the wellhead is gravitation (Figure 15), e.g., the weight of fluid in the well. Below the boiling point, the gravitational pressure difference of the water is about 90 bar/km and it decreases to 13.6 bar/km due to the increasing proportion of steam content in the fluid.

### 6.4 Scaling quantity

There are three simple methods that can be used to assess the calcite scale quantity as was summarized in section 3.3. All these methods are used to estimate the calcite scale quantity for BH6 in the Kangding geothermal field. Because deep fluid sampling was not carried out for this well, the chemical compositions from PHREEQC calculation (Deep water [2]) are used as the initial fluid composition.

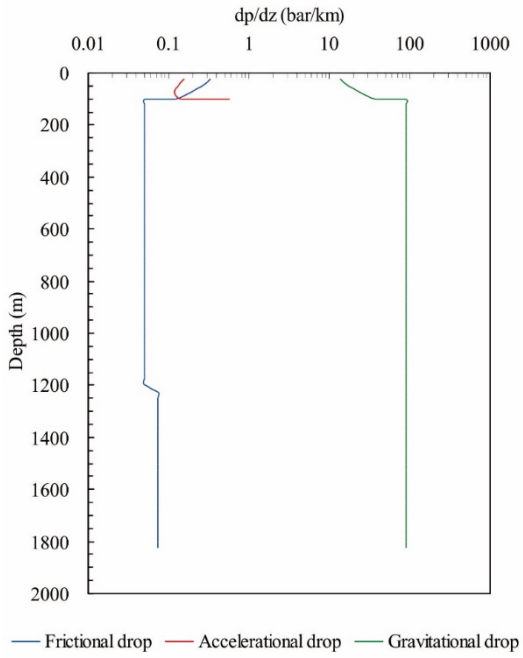


FIGURE 15: Effects of friction, acceleration and gravitation on pressure drop ($CO_2$=0 ppm)

(1) Calculation using the CST method

The reconstructed deep fluid composition using WATCH and PHREEQC is allowed to boil adiabatically at 145°C, 135°C, 125°C and 115°C. The molar ratio of Mg/Ca is calculated to be around 0.21 and thus it may inhibit calcite scaling (Dawe and Zhang, 1997). Because the pH of the solutions changes during boiling from the original 5.6 to 7.7 at the wellhead, Equation 18 which takes into account the influence of both pH and Mg is chosen to calculate the calcite crystal growth rate. The results show that the CST calculated in the well varies from 0 cm to about 2.94 cm for deep fluid (Table 6).

(2) Calculation using calcium difference between the deep fluid and wellhead water

The calcium content of the deep fluid and wellhead water are 44.8 mg/L and 22.0 mg/L, respectively (Table 5). The production rate is about 15.3 kg/s and the discharge time is 48 hours. Therefore, the calcite scale quantity is estimated to be about 151 kg.

(3) Calculation using WATCH and PHREEQC

The reconstructed deep fluid compositions during the boiling process at various temperatures (Table 7) are used as input files in the PHREEQC programme to compute the maximum calcite precipitation quantity. The results in Table 7 show that the calcite scale quantity from the bottom to the wellhead varies from 69.3 mg/kgw to 113.5 mg/kgw. Based on the production rate and discharge time of 15.3 kg/s and 48 hours, respectively, the total quantity of calcite scale is calculated to be 183 kg - 300 kg.

TABLE 6: The CST calculation and calcite scale quantity evaluation based on chemical compositions reconstructed using WATCH and PHREEQC

| T (°C) | pH | Molar ratio of Mg/Ca | Saturation ratio | I (mol/kg) | logKp | Kp | $R_L$ (m/s) | CST (cm) |
|---|---|---|---|---|---|---|---|---|
| 150 | 5.6 | 0.21 | 1.16 | 0.02 | -7.33 | 4.63E-08 | 2.62E-10 | 0 |
| 145 | 6.2 | 0.21 | 4.90 | 0.02 | -7.62 | 2.40E-08 | 3.53E-08 | 0.61 |
| 135 | 7.2 | 0.21 | 29.85 | 0.02 | -8.07 | 8.52E-09 | 1.70E-07 | 2.94 |
| 125 | 7.5 | 0.21 | 47.21 | 0.03 | -8.33 | 4.73E-09 | 1.63E-07 | 2.81 |
| 115 | 7.7 | 0.21 | 59.98 | 0.03 | -8.56 | 2.76E-09 | 1.26E-07 | 2.17 |

TABLE 7: Fluid chemical composition from bottom to wellhead during boiling and calcite scale quantity calculation from PHREEQC simulation

| T (°C) | B | $SiO_2$ | Na | K | Mg | Ca | F | Cl | $SO_4$ | $CO_2$ | $H_2S$ | Al | Fe | Calcite quantity |
|---|---|---|---|---|---|---|---|---|---|---|---|---|---|---|
| | mg/kgw | | | | | | | | | | | µg/kgw | | kg |
| 150 | 2.1 | 128 | 539 | 47.1 | 5.7 | 44.8 | 7.5 | 136 | 15.2 | 7938 | 4.13 | 1.9 | 20 | 0 |
| 145 | 2.1 | 128 | 540 | 47.2 | 5.7 | 44.9 | 7.5 | 136 | 15.2 | 2352 | 2.50 | 1.9 | 20 | 183 |
| 135 | 2.1 | 131 | 551 | 48.2 | 5.8 | 45.8 | 7.7 | 139 | 15.6 | 926 | 1.44 | 1.9 | 20.5 | 280 |
| 125 | 2.2 | 134 | 562 | 49.1 | 5.9 | 46.7 | 7.8 | 142 | 15.9 | 835 | 1.27 | 2 | 20.9 | 292 |
| 115 | 2.2 | 136 | 573 | 50.1 | 6.1 | 47.7 | 8.0 | 145 | 16.2 | 809 | 1.14 | 2 | 21.3 | 300 |

(4) Comparisons of results from different methods

Generally, the results from the calcium difference method and PHREEQC modelling are almost on the same scale, or 151-300 kg, while that from the CST method is from less than 1 cm to 3 cm which is consistent with that observed in the surface pipeline within 48 hours and a flowrate of 15.3 kg/s. Therefore, these three methods can be reliable to some extent.

### 6.5 Scale removal and prevention methods

Calcite scaling problems can be solved from two aspects, removal and prevention. A mechanical scale removal is performed periodically depending on the scaling quantity and it is technically and economically feasible when the operation does not need to be done frequently (e.g., once or twice a year at most). Prevention applies some measures to prevent scale formation before its occurrence.

The main reason for calcite scale formation is a pH increase due to $CO_2$ degassing during the upwelling boiling process. Therefore, there are three ways to prevent scaling: 1) controlling the $CO_2$ partial pressure, 2) altering the pH of the fluid and 3) using chemical additives (inhibitors) (Corsi, 1986). If the geothermal water is just considered for direct use, putting the pump below the boiling depth and cooling the reservoir fluid by injecting cold water based on calcite thermodynamic properties are good methods to avoid calcite scaling (Sverrir Þórhallsson, ISOR, personal communications, 2018).

The $CO_2$ partial pressure can be controlled by down-hole injection of $CO_2$ to maintain high pressure (Kuwada, 1982). However, due to economic feasibility, this procedure is effective only for geothermal fluid with a low $CO_2$ partial pressure. Acid injection can be problematic due to possible corrosion. The high buffering capacity of the geothermal fluid requires large amounts of acid to be injected to lower the pH and the economic cost should be considered (Corsi et al., 1985). Experimental tests carried out in Torre Alfina, Italy indicated that in order to prevent calcite deposition, 200 $cm^3$ of 0.1 N HCl were required per liter of solution, generating high costs (Corsi, 1986). In a geothermal field in South Iceland, sulfuric and hydrochloric acid was injected into the wells below the boiling point to inhibit calcite formation (Ólafsson et al., 2005). The usage of chemical inhibitors thus seems to be the most effective and promising solution for calcite scaling prevention both from technical and economical points of view. Choosing the most suitable inhibitors for a specific geothermal fluid is crucial for effective scale inhibition and the decision should be based on the results of laboratory and field tests.

For the Lihir geothermal field in the Philippines, a polyacrylate based inhibitor and Nalco Scaleguard 84614 were used from 2003 and 2010 respectively to inhibit calcite scaling, both of which were proven to be effective. Because of economic aspects, the latter was chosen for long term usage (Mejorada et al., 2011). For geothermal fields in Turkey with high inorganic carbon content (1.5-3.0 wt. % $CO_2$), organic phosphates and polymeric inhibitors reduced the calcite scale deposition by more than 98% in all boreholes and surface equipment (Yildirim and Yildirim, 2015). A co-polymer of polymaleic anhydrides (PMA) and polyacrylates (PAA) named GEO907 and a combination of PMA and co-polymers alkylether polycarboxylic acid and sulfonates (GEO905) were tested in the Tauhara geothermal field in New Zealand. Results showed that the first one successfully inhibited calcite scaling and helped the production well output to remain steady for 2-3 years while the other one was effective only when using higher dosing concentrations (>30 ppm) (Seastres Jr. et al., 2015). In addition, nano-metal-phosphonates have also been used as an inhibitor to prevent calcite scaling and specific nano-Ca-DTPMP (diethylenetriamine penta (methylenephosphonate)) particles were synthesized and tested. Results showed that they greatly delay the precipitation of calcite by changing the shape and morphology of calcite crystals (Kiaei and Haghtalab, 2014). However, the effectiveness of this kind of inhibitor has to be further tested for geothermal applications.

The process of an inhibitor introduction should include: 1) recognition of the most popular and effective inhibitors available in the market and applied in other geothermal fields; 2) choosing several candidates based on the geochemical characteristics of the fluid and wellhead conditions; 3) testing of these chemicals both in the laboratory and in the field; 4) deciding on one or two inhibitors and including the financial aspects as during the production, the efficiency of the inhibitors may change due to variations in fluid compositions, therefore, long term monitoring is necessary for successful utilization management.

## 7. CONCLUSIONS

The Kangding geothermal field in the west Sichuan Plateau, China is one of the most promising areas for geothermal utilization in the near future. Serious calcite scaling or sinters have been observed in the exploration well BH6 and hot springs around and this is one of the obstacles in high temperature geothermal production in Tibet. The aim of this study is to report the basic geochemical characteristics of $CO_2$ and calcite and assess the calcite scaling potential in the Kangding geothermal field. The main conclusions are presented below:

(1) The deep fluid with a temperature of 150°C-280°C is almost in equilibrium with quartz due to long-term water-rock interactions. The reconstructed reservoir fluid is over-saturated with respect to calcite but it is saturated with respect to quartz and chalcedony.
(2) For wells with calcite scale deposition, precipitated minerals should be considered when reconstructing the reservoir fluid based on wellhead data. Concentrations of elements like Ca and Mg are often under-estimated whereas $CO_2$ content is over-estimated if precipitates are not considered when reconstruct the reservoir fluid using WATCH.
(3) The boiling depth of well BH6 is predicted to be 100-150 m and 440 m without or with $CO_2$ content and salinity considerations, respectively. The higher the $CO_2$ content in the deep fluid, the deeper the boiling depth. The effect of salinity on boiling depth is not as obvious.
(4) The calcite scale quantity is estimated with three methods and ranges from 151 kg to 300 kg or with a thickness of 1-3 cm for the same flow rate and production time. The latter is consistent with the observed scale thickness in the pipeline.
(5) For well BH6, chemical inhibition is suggested as a possible effective method for scale prevention if power generation is considered. The final inhibitor should be chosen based on both laboratory and field tests.

## ACKNOWLEDGEMENTS

I would like to give my great regards to the UNU-GTP that offered me this good opportunity to take the training programme in 2017. I would express my sincere appreciation to Mr. Lúdvík S. Georgsson, Mr. Ingimar G. Haraldsson, Ms Málfríður Ómarsdóttir, Ms Thórhildur Ísberg and Mr. Markús A.G. Wilde, for their assistance and support during these six months in Iceland.

I would also like to thank my supervisor Dr. Iwona Monika Galeczka for her support and sharing of valuable knowledge in the course of my project.

My sincere gratitute also goes to Mr. Finnbogi Óskarsson for his patience and help on sampling and data explanation; Mr. Jón Örn Bjarnason for his nice suggestions on how to use WATCH dealing with samples lacking steam data; Mr. Grimur Bjornsson for teaching me how to use the HOLA program; Mr. Halldór Ármannsson and Mr. Sverrir Þórhallsson for their valuable discussions and experiences on calcite scaling experiences; Ms Rósa S. Jónsdóttir for her help of providing old references and reports for the research project; Ms Christina Günther for her kind explanations on the water and gas analysis. Also, give my best wishes to all the fellows in the UNU-GTP 2017 for our great friendship.

I would also give my great regards to Zhonghe Pang, group members and friends of Tingting Zheng and Donglin Liu who also studied in the Programme, for their support and help.

Finally, I would express my sincere appreciation to my husband Lizhi Zhang, my parents and other family members for their support and patience through my absence from home.

## REFERENCES

Akin, T., Guney, A., and Kargi, H., 2015: Modeling of calcite scaling and estimation of gas breakout depth in a geothermal well by using PHREEQC. *Proceedings of the 40th Workshop on Geothermal Reservoir Engineering, Stanford University, Stanford, CA, US*, 8 pp.

Angus, S., Armstrong, B., and de Reuck, K.M., 1976: *International thermodynamic tables of the fluid state, vol. 3 carbon dioxide*. Pergamon, NY, 385 pp.

Ármannsson, H., 1989: Predicting calcite deposition in Krafla boreholes. *Geothermics, 18-1/2*, 25-32.

Arnórsson, S., 1978: Precipitation of calcite from flashed geothermal waters in Iceland. *Contrib. Mineral. Petrol. 66,* 21-28.

Arnórsson, S., 1981: Mineral deposition from Icelandic geothermal waters, environmental and utilization problems. *J. Petroleum Technology, 33-1,* 181-187.

Arnórsson, S., 1989: Deposition of calcium carbonate minerals from geothermal waters-theoretical considerations. *Geothermics, 18,* 33-39.

Arnórsson, S., Sigurdsson, S. and Svavarsson, H., 1982: The chemistry of geothermal waters in Iceland I. Calculation of aqueous speciation from 0°C to 370°C. *Geochim. Cosmochim. Acta, 46,* 1513-1532.

Atkinson, G., Oklahoma, U., Raju, K., Aramco, S., and Howell, R.D., 1991: The thermodynamics of scale prediction. *SPE 21021*, 209-215.

Bai Liping, 1991: *Chemical modelling programs for predicting calcite scaling, applied to low-temperature geothermal waters in Iceland*. UNU-GTP, Iceland, report 3, 45 pp.

Bénézeth, P., Stefánsson, A., Gautier, Q., and Schott, J., 2013: Mineral solubility and aqueous speciation under hydrothermal conditions to 300°C – the carbonate system as an example. *Reviews in Mineralogy and Geochemistry, 76-1,* 81-133.

Berner, R.A., 1976: The solubility of calcite and aragonite in seawater at one atmosphere and 34.5 parts per thousand. *Am. J. Science, 276*, 713-730.

Bjarnason, J.Ö., 1994: *The speciation program WATCH, version 2.1.* Orkustofnun, Reykjavík, 7 pp.

Björnsson, G. 1987: *A multi-feedzone geothermal wellbore simulator*. University of California., Berkeley, MSc thesis, Lawrence Berkeley Laboratory, report, 102 pp.

Bychkov, A.Yu., Bénézeth, P., Pokrovsky, O.S., Shvarov, Yu., and Schott, J.V., 2007: Experimental determination of calcite solubility and stability at 120-160°C and 2-50 bar $pCO_2$ using in situ pH measurements. *First French-German Symposium on Geological Storage of $CO_2$. Potsdam, Germany. Geotechnologien Science Report 9*, 47-48.

Corsi, R., 1986: Scaling and corrosion in geothermal equipment: problems and preventive measures. *Geothermics, 15*, 839-856.

Corsi, R., Culivicci, G., and Sabatelli, F., 1985: Laboratory and field testing of calcium carbonate scale inhibitors. *Geothermal Resources Council, Transactions*, *9*, 239-244.

Dawe, R. A., and Zhang, Y. 1997: Kinetics of calcium carbonate scaling using observations from glass micro models. *J. Petroleum Science and Engineering*, *18*, 179-187.

Ellis, A.J., 1963: The solubility of calcite in sodium chloride solutions at high temperature. *Amer. J. Sci., 261,* 259-267.

Gledhill, D.K., and Morse, J.W., 2006: Calcite solubility in Na-Ca-Mg-Cl brines. *Chemical Geology, 233*, 249-256.

GSDS, 2017*: GSDS GeoData – GeoData Manager, Steamfield Manager, WellSim*. Geothermal Science and Data Solutions (GSDS), website: *http://www.gsds.co.nz/wellsim-downloads/*.

Gunn, C., and Freeston, D., 1991: An integrated steady-state wellbore simulation and analysis package. *Proceedings of the 13th New Zealand Geothermal Workshop*, Auckland, NZ, 161-166.

Guo, Q., Pang, Z., Wang, Y. and Tian, J. 2017: Fluid geochemistry and geothermometry applications of the Kangding high-temperature geothermal system in eastern Himalayas. *Applied Geochemistry*, *81*, 63-75.

Hu, S.B., He L.J., and Wang J.Y., 2001: Compilation of heat flow data in the China continental area (3rd ed.). *Chinese J. Geophysics, 44*, 611-626 (in Chinese with English abstract).

Iceland Water Chemistry Group, 2010: *The chemical speciation program WATCH, version 2.4*. ÍSOR – Iceland GeoSurvey, Reykjavik, website: *www.geothermal.is/software.*

Izgec, O., Demiral, B., Bertin, H., and Akin, S., 2005: Calcite precipitation in low temperature geothermal systems: an experimental approach. *Proceedings of 30th Workshop on Geothermal Reservoir Engineering, Stanford University, Stanford, Ca,* 6 pp.

Jacobson, R.L., and Langmuir, D., 1974: Dissociation constants of calcite and $CaHCO_3^+$ from 0 to 50°C. *Geochim Cosmochim Acta, 38*, 301-318.

Jiang G.Z., Gao P., and Rao S., 2016: Compilation of heat flow data in the continental area of China (4th ed.). *Chinese J. Geophysics, 59,* 2892-2910.

Kaypakoğlu, B., Şişman, M., and Aksoy, N., 2012: Preventive methods for scaling and corrosion in geothermal fields. *Proceedings of 34th New Zealand Geothermal Workshop, Auckland, NZ*, 6 pp.

Kerrick, D.M. and Jacobs, G.K., 1981: Amodified Redlich-Kwong equation for $H_2O$, $CO_2$ and $H_2O$-$CO_2$ mixtures at elevated pressures and temperatures. *American Journal of Sciences, 281*, 735-767.

Kiaei, Z., and Haghtalab, A., 2014: Experimental study of using Ca-DTPMP nanoparticles in inhibition of $CaCO_3$ scaling in a bulk water process. *Desalination*, *338*, 84-92.

Kuwada, J.T., 1982: Field demonstration of the EFP system for carbonate scale control. *Geothermal Resources Council, Bulletin, 11*, 3-9.

Long X.J., 2014: Application of plateau geothermal well construction technology in Kangding county, Garze prefecture, Sichuan province. *Coal Geology of China, 26-7*, 60-62 +77 (in Chinese with English abstract).

Mejorada, A., Daimol, A., Hermoso, D., Hollams, R., and McCormick, J., 2011: Calcite inhibition system: Lihir experience. *Proceedings of International Workshop on Mineral Scaling, Manila, Philippines*, 93-96.

Nicholson, K.N., 1993: Geothermal fluids. Chemistry and exploration techniques. Springer-Verlag Berlin-Heidelberg, 263 pp.

Ólafsson, M., Hauksdóttir, S., Thórhallsson, S., and Snorrason, T., 2005: Calcite scaling at Selfossveitur hitaveita, S-Iceland, when mixing waters of different chemical composition. *Proceedings of World Geothermal Congress 2005, Antalya, Turkey*, 6 pp.

Quinao, J.J., Buscarlet, E., and Siega, F., 2017: Early identification and management of calcite deposition in the Ngatamariki geothermal field, New Zealand. *Proceedings of the 42nd Workshop on Geothermal Reservoir Engineering, Stanford University, Stanford, Ca*, 9 pp.

Parkhurst, D.L., and Appelo, C.A.J., 1999: *User's guide to PHREEQC (version 2) – A computer program for speciation, batch-reaction, one-dimensional transport, and inverse geochemical calculations*. U.S. Geological Survey, Water-Resources investigations report 97-4259, 312 pp.

Pingtsoe Wangyal, 1992: *Calcite deposition related to temperature and boiling in some Icelandic geothermal wells.* UNU-GTP, Iceland, report 11, 33 pp.

Plummer, L.N., and Busenberg, E., 1982: The solubilities of calcite, aragonite and vaterite in $CO_2$-$H_2O$ solutions between 0 and 90°C, and evaluation of the aqueous model for the system $CaCO_3$-$CO_2$-$H_2O$. *Geochim. Cosmochim. Acta, 46*, 1011-1040.

Rahmani, M.R., 2007: Assessment of calcite scaling potential in the geothermal wells of the NW-Sabalan geothermal prospect, NW-Iran. Report 19 in: *Geothermal training in Iceland in 2007*. UNU-GTP, Iceland, 447-460.

Reed, M.H., Spycher, N.F., and Palandri, J., 2012: *Users' guide for CHIM-XPT: a program for computing reaction processes in aqueous-mineral-gas systems and MINTAB guide (version 2.43).* University of Oregon, Department of Geological Sciences, Eugene, Or USA.

Remoroza, A.I., 2010: *Calcite mineral scaling potential of high-temperature geothermal wells*. University of Iceland, Reykjavík, MSc thesis, 97 pp.

Sass, E., Morse, J.W., and Millero, F.J., 1983: Dependence of the values of calcite and aragonite thermodynamic solubility products on ionic models. *Am. J. Science, 283*, 218- 229.

Segnit, E.R., Holland, H.D., and Biscardi, C.J., 1962: The solubility of calcite in aqueous solutions. I. The solubility of calcite in water between 75 degrees and 200 degrees at $CO_2$ pressures up to 60 atm. *Geochim. Cosmochim. Acta*, *26*: 1301-1331.

Seastres Jr., J., Dean, A., Muller, L., Barrie, K., and Crisford, M., 2015: Borehole testing of calcite dispersion and dissolution chemicals at Tauhara geothermal field, Taupo, New Zealand. *Proceedings of 37th New Zealand Geothermal Workshop, Taupo, New Zealand*, 4 pp.

Sigfússon, B., and Gunnarsson, I., 2011: Scaling prevention experiments in the Hellisheidi power plant, Iceland. *Proceedings of the 36th Workshop on Geothermal Reservoir Engineering, Stanford University, Stanford, California*, 5 pp.

Span, R., and Wagner, W., 1996: A new equation of state for carbon dioxide covering the fluid region from the triple-point temperature to 1100 K at pressures up to 800 MPa. *J. Physical and Chemical Reference Data*, *25-6*, 1509-1596.

Suehiro, Y., Nakajima, M., Yamada, K., and Uematsu, M., 1996: Critical parameters of {x$CO_2$+ (1-x) $CHF_3$} for x=(1.0000, 0.7496, 0.5013, and 0.2522). *J. Chemical Thermodynamics*, *28*, 1153-1164.

Tong, W., and Zhang, M., 1994: *Thermal spring in Hengduan (Traverse) Mountains. The Comprehensive Scientific Expedition to the Qinghai-Xizang Plateau* (in Chinese with English abstract). Science Press, Beijing, 53-60 pp.

Truesdell, A.H., and Fournier, R.O., 1977: Procedure for estimating the temperature of a hot water component in a mixed water using a plot of dissolved silica vs. enthalpy. *U.S. Geol. Survey J. Res., 5,* 49-52.

Villaseñor, L.B., and Calibugan, A.A., 2011: Silica scaling in Tiwi – current solutions. *Proceedings International Workshop on Mineral Scaling 2011, Manila, Philippines*.

Wang Y.X., Liu S.L., Bian Q.Y., Yan B., Liu X.F., Liu J.X., Wang H.Y., and Bu X.B., 2015: Scaling analysis of geothermal well from Ganzi and countermeasures for anti-scale. *Advances in New and Renewable Energy, 3-3,* 202-206 (in Chinese with English abstract).

Wanner, C., Eichinger, F., Jahrfeld, T., and Diamond, L.W., 2017: Causes of abundant calcite scaling in geothermal wells in the Bavarian Molasse Basin, Southern Germany. *Geothermics*, *70*, 324-338.

Wolff-Boenisch, D., and Evans, K., 2013: Geochemical modelling of petroleum well data from the Perth Basin. Implications for potential scaling during low enthalpy geothermal exploration from a hot sedimentary aquifer. *Applied Geochemistry*, *37*, 12-28.

Xu, G., and Kamp, P.J., 2000: Tectonics and denudation adjacent to the Xianshuihe fault, eastern Tibetan Plateau: constraints from fission track thermochronology. *J. Geophysics Research - Solid Earth, 105-B8*, 19231–19251.

Xu Z., Yang J., Li H., Ji S., Zhang Z., and Liu Y., 2011: On the tectonics of the India-Asia Collision. *Acta Geol. Sin., 85-1*, 1–33 (in Chinese with English abstract).

Yildirim, N., and Yildirim, A., 2015: High total inorganic carbon concentration, dependent carbonate scaling and mitigation system, in moderate to high enthalpy geothermal fields in Turkey. *Proceedings of the World Geothermal Congress 2015, Melbourne Australia,* 7 pp.

Zhang H., Hu Y.Z., Yun Z.H., and Qu Z.W., 2016: Applying hydro-geochemistry simulating technology to study scaling of the high-temperature geothermal well in Kangding Couty. *Advances in New and Renewable Energy, 4-2*, 111-117 (in Chinese with English abstract).

Zhang, Y., and Dawhe, R., 1998: The kinetics of calcite precipitation from a high salinity water. *Applied Geochemistry, 13/2*, 177-184.

Zhang, Y., and Farquhar, R., 2001: Laboratory determination of calcium carbonate scaling rates for oilfield wellbore environments. *Proceedings of International Symposium on Oilfield* Scale. Society of Petroleum Engineers.

Zhang, Y., Shaw, H., Farquhar, R., and Dawe, R., 2001: The kinetics of carbonate scaling - application for the prediction of down hole carbonate scaling. *J. Petroleum Science and Engineering*, *29-2,* 85-95.

**APPENDIX I: Boiling depth calculated using HOLA program without $CO_2$ consideration**

| Depth (m) | Pressure (bar-a) | Temp (°C) | Dryness (%) | $H_w$ | $H_s$ | $H_t$ (kJ/kg) | $V_w$ | $V_s$ (m/s) | $D_w$ | $D_s$ ($kg/m^3$) | Rad (mm) | Reg |
|---|---|---|---|---|---|---|---|---|---|---|---|---|
| 0 | 1.9 | 118.6 | 5.3 | 498 | 2704 | 615 | 9.14 | 20.77 | 943.9 | 1.1 | 110 | Sl |
| 25 | 2.1 | 121.4 | 4.8 | 510 | 2708 | 615 | 7.71 | 17.46 | 941.7 | 1.2 | 110 | Sl |
| 50 | 2.3 | 124.2 | 4.3 | 522 | 2712 | 616 | 6.44 | 14.51 | 939.4 | 1.3 | 110 | Sl |
| 75 | 2.5 | 127.2 | 3.7 | 534 | 2716 | 616 | 5.26 | 11.79 | 936.9 | 1.4 | 110 | Sl |
| 100 | 2.7 | 130.5 | 3.1 | 548 | 2721 | 616 | 4.13 | 9.21 | 934.2 | 1.5 | 110 | Sl |
| 125 | 3.1 | 134.3 | 2.4 | 565 | 2726 | 616 | 2.99 | 6.63 | 930.9 | 1.7 | 110 | Sl |
| 150 | 3.6 | 140.1 | 1.3 | 590 | 2733 | 617 | 1.59 | 3.50 | 925.8 | 2.0 | 110 | Sl |
| 175 | 5.9 | 146.4 | 0 | 617 | 0 | 617 | 0.44 | 0 | 920.2 | 0 | 110 | 1p |
| 200 | 8.2 | 146.4 | 0 | 617 | 0 | 617 | 0.44 | 0 | 920.3 | 0 | 110 | 1p |
| 225 | 10.4 | 146.5 | 0 | 617 | 0 | 617 | 0.44 | 0 | 920.4 | 0 | 110 | 1p |
| 250 | 12.7 | 146.5 | 0 | 618 | 0 | 618 | 0.44 | 0 | 920.5 | 0 | 110 | 1p |
| 275 | 14.9 | 146.5 | 0 | 618 | 0 | 618 | 0.44 | 0 | 920.6 | 0 | 110 | 1p |
| 300 | 17.2 | 146.5 | 0 | 618 | 0 | 618 | 0.44 | 0 | 920.7 | 0 | 110 | 1p |
| 325 | 19.5 | 146.6 | 0 | 618 | 0 | 618 | 0.44 | 0 | 920.8 | 0 | 110 | 1p |
| 350 | 21.7 | 146.6 | 0 | 618 | 0 | 618 | 0.44 | 0 | 920.9 | 0 | 110 | 1p |
| 375 | 24.0 | 146.6 | 0 | 619 | 0 | 619 | 0.44 | 0 | 921.0 | 0 | 110 | 1p |
| 400 | 26.2 | 146.6 | 0 | 619 | 0 | 619 | 0.44 | 0 | 921.1 | 0 | 110 | 1p |
| 425 | 28.5 | 146.6 | 0 | 619 | 0 | 619 | 0.44 | 0 | 921.3 | 0 | 110 | 1p |
| 450 | 30.8 | 146.7 | 0 | 619 | 0 | 619 | 0.44 | 0 | 921.4 | 0 | 110 | 1p |
| 475 | 33.0 | 146.7 | 0 | 620 | 0 | 620 | 0.44 | 0 | 921.5 | 0 | 110 | 1p |
| 500 | 35.3 | 146.7 | 0 | 620 | 0 | 620 | 0.44 | 0 | 921.6 | 0 | 110 | 1p |
| 525 | 37.5 | 146.7 | 0 | 620 | 0 | 620 | 0.44 | 0 | 921.7 | 0 | 110 | 1p |
| 550 | 39.8 | 146.8 | 0 | 620 | 0 | 620 | 0.44 | 0 | 921.8 | 0 | 110 | 1p |
| 575 | 42.1 | 146.8 | 0 | 621 | 0 | 621 | 0.44 | 0 | 921.9 | 0 | 110 | 1p |
| 600 | 44.3 | 146.8 | 0 | 621 | 0 | 621 | 0.44 | 0 | 922 | 0 | 110 | 1p |
| 700 | 53.4 | 146.9 | 0 | 622 | 0 | 622 | 0.44 | 0 | 922.4 | 0 | 110 | 1p |
| 800 | 62.4 | 147.0 | 0 | 623 | 0 | 623 | 0.44 | 0 | 922.9 | 0 | 110 | 1p |
| 900 | 71.5 | 147.1 | 0 | 624 | 0 | 624 | 0.44 | 0 | 923.3 | 0 | 110 | 1p |
| 1000 | 80.6 | 147.2 | 0 | 625 | 0 | 625 | 0.44 | 0 | 923.7 | 0 | 110 | 1p |
| 1100 | 89.6 | 147.3 | 0 | 626 | 0 | 626 | 0.44 | 0 | 924.1 | 0 | 110 | 1p |
| 1200 | 98.7 | 147.4 | 0 | 627 | 0 | 627 | 0.44 | 0 | 924.5 | 0 | 110 | 1p |
| 1300 | 107.8 | 147.5 | 0 | 628 | 0 | 628 | 0.53 | 0 | 925 | 0 | 100 | 1p |
| 1400 | 116.9 | 147.6 | 0 | 629 | 0 | 629 | 0.53 | 0 | 925.4 | 0 | 100 | 1p |
| 1500 | 126.0 | 147.7 | 0 | 630 | 0 | 630 | 0.53 | 0 | 925.8 | 0 | 100 | 1p |
| 1600 | 135.1 | 147.8 | 0 | 631 | 0 | 631 | 0.53 | 0 | 926.2 | 0 | 100 | 1p |
| 1700 | 144.2 | 147.9 | 0 | 632 | 0 | 632 | 0.53 | 0 | 926.6 | 0 | 100 | 1p |
| 1800 | 153.3 | 147.9 | 0 | 633 | 0 | 633 | 0.53 | 0 | 927 | 0 | 100 | 1p |
| 1825 | 155.5 | 148.0 | 0 | 633 | 0 | 633 | 0.53 | 0 | 927.1 | 0 | 100 | 1p |
| 1850 | 157.8 | 148.0 | 0 | 633 | 0 | 633 | 0.53 | 0 | 927.2 | 0 | 100 | 1p |

**APPENDIX II: Boiling depth calculated using WELLSIM program without $CO_2$ consideration**

| Depth (m) | Pressure (bars-a) | Temperature (°C) | $H_t$ (kJ/kg) | Dryness (%) | $C_{CO2}$ (ppm) | $P_{CO2}$ bar-a | $V_w$ (m/s) | $V_s$ (m/s) | Regime |
|---|---|---|---|---|---|---|---|---|---|
| 0 | 1.2 | 118.7 | 615.0 | 5.3 | 0 | 0.01 | 3.0 | 21.4 | Annular |
| 25 | 1.6 | 124.1 | 615.2 | 4.3 | 0 | 0.01 | 2.4 | 16.1 | Annular |
| 50 | 2.0 | 130.0 | 615.5 | 3.2 | 0 | 0.01 | 1.9 | 10.8 | Annular |
| 75 | 2.6 | 136.8 | 615.7 | 1.9 | 0 | 0.01 | 1.3 | 6.0 | Churn |
| 100 | 3.5 | 145.6 | 616.0 | 0.2 | 0 | 0.01 | 0.6 | 1.0 | Bubble |
| 101 | 3.6 | 146.4 | 616.0 | 0 | 0 | 0.01 | 0.4 | 0 | Flash |
| 126 | 5.9 | 146.4 | 616.2 | 0 | 0 | 0.01 | 0.4 | 0 | Liquid |
| 151 | 8.1 | 146.5 | 616.5 | 0 | 0 | 0.01 | 0.4 | 0 | Liquid |
| 176 | 10.4 | 146.5 | 616.7 | 0 | 0 | 0.01 | 0.4 | 0 | Liquid |
| 201 | 12.7 | 146.6 | 617.0 | 0 | 0 | 0.01 | 0.4 | 0 | Liquid |
| 226 | 14.9 | 146.7 | 617.2 | 0 | 0 | 0.01 | 0.4 | 0 | Liquid |
| 251 | 17.2 | 146.7 | 617.5 | 0 | 0 | 0.01 | 0.4 | 0 | Liquid |
| 276 | 19.5 | 146.8 | 617.7 | 0 | 0 | 0.01 | 0.4 | 0 | Liquid |
| 301 | 21.7 | 146.8 | 618.0 | 0 | 0 | 0.01 | 0.4 | 0 | Liquid |
| 326 | 24.0 | 146.9 | 618.2 | 0 | 0 | 0.01 | 0.4 | 0 | Liquid |
| 351 | 26.3 | 146.9 | 618.4 | 0 | 0 | 0.01 | 0.4 | 0 | Liquid |
| 376 | 28.5 | 147.0 | 618.7 | 0 | 0 | 0.01 | 0.4 | 0 | Liquid |
| 401 | 30.8 | 147.1 | 618.9 | 0 | 0 | 0.01 | 0.4 | 0 | Liquid |
| 426 | 33.1 | 147.1 | 619.2 | 0 | 0 | 0.01 | 0.4 | 0 | Liquid |
| 451 | 35.3 | 147.2 | 619.4 | 0 | 0 | 0.01 | 0.4 | 0 | Liquid |
| 476 | 37.6 | 147.2 | 619.7 | 0 | 0 | 0.01 | 0.4 | 0 | Liquid |
| 501 | 39.9 | 147.3 | 619.9 | 0 | 0 | 0.01 | 0.4 | 0 | Liquid |
| 526 | 42.1 | 147.3 | 620.2 | 0 | 0 | 0.01 | 0.4 | 0 | Liquid |
| 551 | 44.4 | 147.4 | 620.4 | 0 | 0 | 0.01 | 0.4 | 0 | Liquid |
| 576 | 46.7 | 147.5 | 620.7 | 0 | 0 | 0.01 | 0.4 | 0 | Liquid |
| 601 | 49.0 | 147.5 | 620.9 | 0 | 0 | 0.01 | 0.4 | 0 | Liquid |
| 701 | 58.0 | 147.7 | 621.9 | 0 | 0 | 0.01 | 0.4 | 0 | Liquid |
| 801 | 67.1 | 148.0 | 622.9 | 0 | 0 | 0.01 | 0.4 | 0 | Liquid |
| 901 | 76.2 | 148.2 | 623.8 | 0 | 0 | 0.01 | 0.4 | 0 | Liquid |
| 1001 | 85.3 | 148.4 | 624.8 | 0 | 0 | 0.01 | 0.4 | 0 | Liquid |
| 1101 | 94.4 | 148.6 | 625.8 | 0 | 0 | 0.01 | 0.4 | 0 | Liquid |
| 1200 | 103.4 | 148.9 | 626.8 | 0 | 0 | 0.01 | 0.4 | 0 | Liquid |
| 1300 | 112.5 | 149.1 | 627.8 | 0 | 0 | 0.01 | 0.5 | 0 | Liquid |
| 1400 | 121.6 | 149.3 | 628.7 | 0 | 0 | 0.01 | 0.5 | 0 | Liquid |
| 1500 | 130.7 | 149.6 | 629.7 | 0 | 0 | 0.01 | 0.5 | 0 | Liquid |
| 1600 | 139.8 | 149.8 | 630.7 | 0 | 0 | 0.01 | 0.5 | 0 | Liquid |
| 1700 | 148.9 | 150.0 | 631.7 | 0 | 0 | 0.01 | 0.5 | 0 | Liquid |
| 1800 | 158.0 | 150.2 | 632.7 | 0 | 0 | 0.01 | 0.5 | 0 | Liquid |
| 1825 | 160.3 | 150.3 | 632.9 | 0 | 0 | 0.01 | 0.5 | 0 | Liquid |

**APPENDIX III: Boiling depth calculated using WELLSIM program with $CO_2$ content of 2352 ppm**

| Depth (m) | Pressure (bars-a) | Temperature (°C) | $H_t$ (kJ/kg) | Dryness (%) | C $_{CO2}$ (ppm) | P $_{CO2}$ Bar-a | $V_w$ (m/s) | $V_s$ (m/s) | Regime |
|---|---|---|---|---|---|---|---|---|---|
| 0 | 1.9 | 118.2 | 615.0 | 5.6 | 2352 | 0.04 | 3.0 | 22.1 | Annular |
| 25 | 2.2 | 123.3 | 615.2 | 4.7 | 2352 | 0.05 | 2.5 | 17.0 | Annular |
| 50 | 2.7 | 128.7 | 615.5 | 3.7 | 2352 | 0.08 | 2.0 | 11.8 | Annular |
| 75 | 3.2 | 134.5 | 615.7 | 2.6 | 2352 | 0.13 | 1.5 | 7.5 | Churn |
| 100 | 3.9 | 140.3 | 616.0 | 1.5 | 2352 | 0.28 | 1.1 | 3.9 | Churn |
| 125 | 4.9 | 144.4 | 616.2 | 0.6 | 2352 | 0.83 | 0.7 | 1.7 | Slug |
| 150 | 6.3 | 145.8 | 616.5 | 0.3 | 2352 | 2.00 | 0.6 | 0.8 | Bubble |
| 175 | 8.1 | 146.4 | 616.7 | 0.1 | 2352 | 3.75 | 0.5 | 0.8 | Bubble |
| 200 | 10.3 | 146.6 | 617.0 | 0.0 | 2352 | 5.81 | 0.4 | 0.7 | Bubble |
| 204 | 10.7 | 146.7 | 617.0 | 0 | 2352 | 6.17 | 0.4 | 0.0 | Flash |
| 229 | 12.9 | 146.7 | 617.2 | 0 | 2352 | 6.17 | 0.4 | 0.0 | Liquid |
| 254 | 15.2 | 146.8 | 617.5 | 0 | 2352 | 6.17 | 0.4 | 0.0 | Liquid |
| 279 | 17.5 | 146.8 | 617.7 | 0 | 2352 | 6.17 | 0.4 | 0.0 | Liquid |
| 304 | 19.8 | 146.9 | 618.0 | 0 | 2352 | 6.17 | 0.4 | 0.0 | Liquid |
| 329 | 22.0 | 147.0 | 618.2 | 0 | 2352 | 6.17 | 0.4 | 0.0 | Liquid |
| 354 | 24.3 | 147.0 | 618.5 | 0 | 2352 | 6.17 | 0.4 | 0.0 | Liquid |
| 379 | 26.6 | 147.1 | 618.7 | 0 | 2352 | 6.17 | 0.4 | 0.0 | Liquid |
| 404 | 28.8 | 147.1 | 619.0 | 0 | 2352 | 6.17 | 0.4 | 0.0 | Liquid |
| 429 | 31.1 | 147.2 | 619.2 | 0 | 2352 | 6.17 | 0.4 | 0.0 | Liquid |
| 454 | 33.4 | 147.2 | 619.5 | 0 | 2352 | 6.17 | 0.4 | 0.0 | Liquid |
| 479 | 35.7 | 147.3 | 619.7 | 0 | 2352 | 6.17 | 0.4 | 0.0 | Liquid |
| 504 | 37.9 | 147.4 | 619.9 | 0 | 2352 | 6.17 | 0.4 | 0.0 | Liquid |
| 529 | 40.2 | 147.4 | 620.2 | 0 | 2352 | 6.17 | 0.4 | 0.0 | Liquid |
| 604 | 47.0 | 147.6 | 620.9 | 0 | 2352 | 6.17 | 0.4 | 0.0 | Liquid |
| 704 | 56.1 | 147.8 | 621.9 | 0 | 2352 | 6.18 | 0.4 | 0.0 | Liquid |
| 804 | 65.2 | 148.0 | 622.9 | 0 | 2352 | 6.18 | 0.4 | 0.0 | Liquid |
| 904 | 74.3 | 148.3 | 623.9 | 0 | 2352 | 6.18 | 0.4 | 0.0 | Liquid |
| 1004 | 83.4 | 148.5 | 624.8 | 0 | 2352 | 6.18 | 0.4 | 0.0 | Liquid |
| 1104 | 92.5 | 148.7 | 625.8 | 0 | 2352 | 6.18 | 0.4 | 0.0 | Liquid |
| 1200 | 101.2 | 148.9 | 626.8 | 0 | 2352 | 6.19 | 0.4 | 0.0 | Liquid |
| 1300 | 110.4 | 149.2 | 627.8 | 0 | 2352 | 6.19 | 0.5 | 0.0 | Liquid |
| 1400 | 119.5 | 149.4 | 628.7 | 0 | 2352 | 6.19 | 0.5 | 0.0 | Liquid |
| 1500 | 128.6 | 149.6 | 629.7 | 0 | 2352 | 6.19 | 0.5 | 0.0 | Liquid |
| 1525 | 130.9 | 149.7 | 630.0 | 0 | 2352 | 6.19 | 0.5 | 0.0 | Liquid |
| 1550 | 133.2 | 149.7 | 630.2 | 0 | 2352 | 6.19 | 0.5 | 0.0 | Liquid |
| 1575 | 135.4 | 149.8 | 630.5 | 0 | 2352 | 6.19 | 0.5 | 0.0 | Liquid |
| 1600 | 137.7 | 149.9 | 630.7 | 0 | 2352 | 6.19 | 0.5 | 0.0 | Liquid |
| 1700 | 146.8 | 150.1 | 631.7 | 0 | 2352 | 6.19 | 0.5 | 0.0 | Liquid |
| 1800 | 156.0 | 150.3 | 632.7 | 0 | 2352 | 6.20 | 0.5 | 0.0 | Liquid |
| 1825 | 158.3 | 150.4 | 632.9 | 0 | 2352 | 6.20 | 0.5 | 0.0 | Liquid |

## APPENDIX IV: Boiling depth calculated using WELLSIM program with $CO_2$ content of 7938 ppm

| Depth (m) | Pressure (bars-a) | Temperature (°C) | $H_t$ (kJ/kg) | Dryness (%) | C $_{CO2}$ (ppm) | P $_{CO2}$ bar-a | $V_w$ (m/s) | $V_s$ (m/s) | Regime |
|---|---|---|---|---|---|---|---|---|---|
| 0 | 1.9 | 116.9 | 615.0 | 6.3 | 7938 | 0.11 | 3.2 | 24.2 | Annular |
| 10 | 2.0 | 118.8 | 615.1 | 6.0 | 7938 | 0.13 | 3.0 | 22.0 | Annular |
| 20 | 2.2 | 120.6 | 615.2 | 5.7 | 7938 | 0.14 | 2.8 | 19.7 | Annular |
| 30 | 2.3 | 122.5 | 615.3 | 5.3 | 7938 | 0.16 | 2.6 | 17.5 | Annular |
| 40 | 2.4 | 124.4 | 615.4 | 5.0 | 7938 | 0.18 | 2.4 | 15.6 | Annular |
| 50 | 2.6 | 126.2 | 615.5 | 4.6 | 7938 | 0.21 | 2.3 | 13.8 | Annular |
| 90 | 3.4 | 133.7 | 615.9 | 3.2 | 7938 | 0.40 | 1.6 | 7.8 | Annular |
| 100 | 3.7 | 135.5 | 616.0 | 2.9 | 7938 | 0.49 | 1.4 | 6.6 | Churn |
| 150 | 5.3 | 142.1 | 616.5 | 1.6 | 7938 | 1.42 | 1.0 | 2.8 | Churn |
| 170 | 6.1 | 143.5 | 616.7 | 1.3 | 7938 | 2.11 | 0.8 | 2.0 | Churn |
| 180 | 6.6 | 144.0 | 616.8 | 1.2 | 7938 | 2.52 | 0.8 | 1.8 | Slug |
| 190 | 7.1 | 144.4 | 616.9 | 1.1 | 7938 | 2.94 | 0.8 | 1.5 | Slug |
| 200 | 7.6 | 144.7 | 617.0 | 1.0 | 7938 | 3.40 | 0.7 | 1.4 | Slug |
| 210 | 8.1 | 145.0 | 617.1 | 0.9 | 7938 | 3.89 | 0.7 | 1.2 | Slug |
| 240 | 9.9 | 145.5 | 617.4 | 0.8 | 7938 | 5.51 | 0.6 | 0.9 | Slug |
| 250 | 10.5 | 145.7 | 617.5 | 0.7 | 7938 | 6.09 | 0.6 | 0.9 | Bubble |
| 290 | 13.3 | 146.1 | 617.8 | 0.6 | 7938 | 8.77 | 0.5 | 0.9 | Bubble |
| 300 | 14.0 | 146.2 | 617.9 | 0.5 | 7938 | 9.49 | 0.5 | 0.8 | Bubble |
| 340 | 17.2 | 146.5 | 618.3 | 0.4 | 7938 | 12.55 | 0.5 | 0.8 | Bubble |
| 350 | 18.1 | 146.5 | 618.4 | 0.3 | 7938 | 13.35 | 0.5 | 0.8 | Bubble |
| 380 | 20.6 | 146.7 | 618.7 | 0.2 | 7938 | 15.81 | 0.4 | 0.8 | Bubble |
| 420 | 24.1 | 146.9 | 619.1 | 0.1 | 7938 | 19.20 | 0.4 | 0.7 | Bubble |
| 440 | 25.9 | 146.9 | 619.3 | 0.0 | 7938 | 20.94 | 0.4 | 0.7 | Bubble |
| 447 | 26.6 | 147.0 | 619.4 | 0.0 | 7938 | 21.55 | 0.4 | 0.0 | Flash |
| 457 | 27.5 | 147.0 | 619.5 | 0.0 | 7938 | 21.55 | 0.4 | 0.0 | Liquid |
| 507 | 32.0 | 147.1 | 620.0 | 0.0 | 7938 | 21.56 | 0.4 | 0.0 | Liquid |
| 607 | 41.1 | 147.3 | 621.0 | 0.0 | 7938 | 21.56 | 0.4 | 0.0 | Liquid |
| 707 | 50.2 | 147.6 | 621.9 | 0.0 | 7938 | 21.57 | 0.4 | 0.0 | Liquid |
| 807 | 59.3 | 147.8 | 622.9 | 0.0 | 7938 | 21.57 | 0.4 | 0.0 | Liquid |
| 907 | 68.5 | 148.0 | 623.9 | 0.0 | 7938 | 21.58 | 0.4 | 0.0 | Liquid |
| 1007 | 77.6 | 148.2 | 624.9 | 0.0 | 7938 | 21.58 | 0.4 | 0.0 | Liquid |
| 1107 | 86.7 | 148.5 | 625.9 | 0.0 | 7938 | 21.59 | 0.4 | 0.0 | Liquid |
| 1200 | 95.2 | 148.7 | 626.8 | 0.0 | 7938 | 21.59 | 0.4 | 0.0 | Liquid |
| 1300 | 104.3 | 148.9 | 627.8 | 0.0 | 7938 | 21.60 | 0.5 | 0.0 | Liquid |
| 1400 | 113.4 | 149.1 | 628.7 | 0.0 | 7938 | 21.60 | 0.5 | 0.0 | Liquid |
| 1500 | 122.6 | 149.4 | 629.7 | 0.0 | 7938 | 21.60 | 0.5 | 0.0 | Liquid |
| 1600 | 131.7 | 149.6 | 630.7 | 0.0 | 7938 | 21.61 | 0.5 | 0.0 | Liquid |
| 1700 | 140.8 | 149.8 | 631.7 | 0.0 | 7938 | 21.61 | 0.5 | 0.0 | Liquid |
| 1800 | 150.0 | 150.1 | 632.7 | 0.0 | 7938 | 21.62 | 0.5 | 0.0 | Liquid |
| 1825 | 152.3 | 150.1 | 632.9 | 0.0 | 7938 | 21.62 | 0.5 | 0.0 | Liquid |